Implications of ~~D~~differences between recent anthropogenic aerosol emission inventories on diagnosed ~~strongly affect anthropogenic aerosol evolution~~AOD and radiative forcing from 1990 to 2019

Marianne T. Lund[1,*], Gunnar Myhre[1], Ragnhild B. Skeie[1], Bjørn H. Samset[1], Zbigniew Klimont[2]

1 CICERO Center for International Climate Research, Oslo, Norway

2 International Institute for Applied Systems Analysis (IIASA), Laxenburg, Austria

Corresponding author: m.t.lund@cicero.oslo.no

Abstract

This study focuses on implications of differences between recent global emissions inventories for simulated trends in anthropogenic aerosol abundances and radiative forcing (RF) over the 1990-2019 period. We use the ECLIPSE version 6 (ECLv6) and Community Emission Data System year 2021 release (CEDS21) as input to the chemical transport model OsloCTM3 and compare the resulting aerosol evolution to corresponding results derived with the first CEDS release, as well as to observed trends in regional and global aerosol optical depth (AOD). Using CEDS21 and ECLv6 results in 3% and 6% lower global mean AOD compared to CEDS in 2014, primarily driven by differences over China and India, where the area average AOD is up to 30% lower. These differences are considerably larger than the satellite-derived interannual variability in AOD. A negative linear trend (over 2005-2017) in global AOD following changes in anthropogenic emissions is found with all three inventories but is markedly stronger with CEDS21 and ECLv6. Furthermore, we confirm that the model better captures the sign and strength of the observed AOD trend over China with CEDS21 and ECLv6 compared to using CEDS, while the opposite is the case for South Asia. We estimate a net, global mean aerosol-induced RF in 2014 relative to 1990 of 0.08 W m^{-2} for CEDS21, and 0.12 W m^{-2} for ECLv6, compared to 0.03 W m^{-2} with CEDS. Using CEDS21, we also estimate the RF in 2019 relative to 1990 to be 0.10 W m^{-2}, reflecting the continuing decreasing trend in aerosol loads post 2014. Our results facilitate more rigorous comparison between existing and upcoming studies of climate and health effects of aerosols using different emission inventories.

1 Introduction

Human activities have led to a substantial increase in atmospheric abundances of aerosols relative to pre-industrial conditions. While increasing emissions of greenhouse gases is the dominant driver of recent global warming, aerosols play a key role in shaping regional and global climate, and for anthropogenic climate change, through their interactions with radiation and clouds. The sixth assessment report (AR6) of the Intergovernmental Panel on Climate Change (IPCC) estimates that changes in atmospheric aerosols have contributed an effective radiative forcing (ERF) of –1.3 W m^{-2} over the industrial era (1750–2014), albeit with a wide uncertainty range of –2.0 to –0.6 W m^{-2} (Forster et al., 2021).

Over recent decades, anthropogenic emissions of aerosols and their precursor gases ha~~s been~~ve changed~~ing~~ rapidly, with substantial spatiotemporal heterogeneity, ~~and~~ particularly in Asia. Following decades of rapid economic growth in China, the combustion of coal, other fossil fuels, and biofuels increased considerably, resulting in the region becoming the dominan~~ting~~t source of air pollution

emissions. However, since the ~~implementation~~ adoption of the national a~~A~~ction p~~P~~lans targeting particulate matter levels (i.e. ~~on~~ Air Pollution Prevention and Control in 2013 (SCPRC, 2013) and Winning the Blue Sky Defense Battle in 2018 (SCPRC, 2018)), emissions of sulfur dioxide (SO_2) and then nitrogen oxide (NOx) in China have declined rapidly (Klimont et al., 2017; Klimont et al., 2013; Tong et al., 2020; Zheng et al., 2018). Recent studies suggest that also black carbon (BC) emissions are declining (Kanaya et al., 2020; Zheng et al., 2018). ~~In contrast, a~~A ~~continuing~~ strong growth in emissions of SO_2 and other pollutants ~~emissions~~ has been seen in South Asia (Kurokawa & Ohara, 2020), resulting, according to studies, in India overtaking China as the dominant emitter of SO_2 (Li et al., 2017). These contrasting trends have given rise to a distinct dipole pattern of increasing and declining aerosol optical depth over South and East Asia, respectively, visible in satellite data (Samset et al., 2019). Such rapid ~~aerosol~~ changes are likely to affect the climate of the region~~sal climate~~, as aerosols have been shown to have a notable influence on regional temperature and precipitation, including extremes (e.g. Bollasina et al., 2011; Hegerl et al., 2019; Marvel et al., 2020; Samset et al., 2018; Sillmann et al., 2013), with different responses to scattering and absorbing aerosols. H~~h~~owever, the exact nature and magnitude of such climate implications ~~magnitude and role~~ need to better quantified (Persad et al., 2022)~~remains insufficiently quantified~~. ~~However, the overall scientific uncertainty on aerosol induced global mean radiative forcing is still larger than the estimated regional changes , and also varies over the recent decades depending on the overall level of emissions and their location relative to cloud decks and other climate features.~~

Robust quantification of the impacts of aerosols requires reliable and consistent estimates of anthropogenic emissions. However, currently there exist ~~One factor contributing to uncertainty is the~~ substantial differences, in both magnitudes and trends, ~~that exist~~ between available ~~current~~ emission inventories (e.g. Crippa et al., 2018; Elguindi et al., 2020; Smith et al., 2022). Emission inventories are quantifications of contributions from various industrial processes or other anthropogenic activities to the rate of emissions of various compounds to the atmosphere. They generally combine bottom-up information such as reported economic activities with direct observations and process modelling and are used extensively in essentially all efforts to quantify climate and air quality implications of human activities. While the overall scientific uncertainty on aerosol-induced global mean radiative forcing (RF) is larger than the estimated regional changes, the uncertainty also varies over the recent decades depending on the overall level of emissions and their location relative to cloud decks and other climate features (Bellouin et al., 2020; Regayre et al., 2014; Samset et al., 2019; Szopa et al., 2021). Hence, understanding both the inherent inventory differences and the implications of these on downstream calculations and modelled quantities such as aerosol optical depths and radiative forcing is crucial.

As an example, a critical issue that has recently been highlighted is a notable underestimation of the decline in Chinese emissions of SO_2 and NOx, and overestimation of carbonaceous aerosol emissions in Asia and Africa, in the Community Emission Data System (CEDS) developed for the sixth cycle of the Coupled Model Intercomparison Project (CMIP6) (Szopa et al., 2021). Recent work has shown that results from the CMIP6 experiments fail to fully capture the observed recent trends in aerosol optical depth (AOD) in Asia (Cherian & Quaas, 2020; Ramachandran et al., 2022; Su et al., 2021; Wang et al., 2021), with the discrepancy largely attributed to the misrepresentation of emissions in the region in last decade of the historical CMIP6 period. Other studies demonstrate that the poor representation of observed aerosol trends can propagate to further uncertainties in attribution of aerosol-induced impacts, such as the East Asian monsoon (Wang et al., 2022) and health impacts (Cheng et al., 2021). In addition to CMIP6, the CEDS emissions have also been used in individual model studies of historical aerosol evolution, radiative forcing, sector attribution, and air quality assessments (e.g. Bauer et al., 2020; Chowdhury et al., 2022; Lund et al., 2018; Lund et al., 2020; Paulot et al., 2018). Moreover, uncertainties and biases in the baseline historical inventory may influence scenario-based assessments of near-term future regional climate risk.

Since the initial parts of the CMIP6 exercise, the CEDS inventory has undergone several revisions. The most recent version from 2021, ~~CEDS21~~, covering the period up to 2019, exhibit several key differences compared to the initial release – for some species all the way back to the early 2000s ~~(O'Rourke et al. (2021))~~. More specifically, ~~In particular, both~~ emissions of BC, ~~and~~ OC and NOx are ~~emissions are~~all substantially lower in the update, in global totals and, particularly, in Asia, and ~~issues related to~~ the decreasing trend in Chinese SO_2 is more pronounced~~are largely addressed~~. However, the implications of these differences in input data on simulated anthropogenic aerosol distributions, globally and regionally, and the resulting radiative forcing, are not fully quantified and cannot be directly extrapolated. Furthermore,

~~Given the relative importance of these source regions, such inventory differences may have implications for simulations of anthropogenic aerosol distributions globally and contribute to increased uncertainty in estimates of aerosol-induced climate impacts, both in the IPCC AR6 and elsewhere in the literature. For instance, recent work has shown that results from the CMIP6 experiments fail to fully capture the observed recent trends in aerosol optical depth (AOD) in Asia (Cherian & Quaas, 2020; Ramachandran et al., 2022; Su et al., 2021; Wang et al., 2021), with the discrepancy largely attributed to the misrepresentation of emissions in the region in last decade of the historical CMIP6 period. Other studies demonstrate that the poor representation of observed aerosol trends can propagate to further uncertainties in attribution of aerosol-induced impacts, such as the East Asian monsoon (Wang et al., 2022) and health impacts (Cheng et al., 2021). In addition to CMIP6, the CEDS emissions have also been used in individual model studies of historical aerosol evolution, radiative forcing, sector attribution, and air quality assessments (e.g. Bauer et al., 2020; Chowdhury et al., 2022; Lund et al., 2018; Lund et al., 2020; Paulot et al., 2018). Moreover, uncertainties and biases in the baseline historical inventory may influence scenario-based assessments of near-term future regional climate risk.~~

~~A~~as the update to CEDS came too late for uptake in IPCC AR6, it is pertinent to ask ~~investigate~~if the influence of these emission inventory differences affected t~~on t~~he assessed ~~modeled~~ evolution of atmospheric aerosol trends and subsequent climate implications.

Here, we present ~~undertake one~~ an ~~such i~~investigation of the implications of known differences in recent emission inventories on quantified aerosol burdens, optical depth, and radiative forcing, over the period 1990-2019. Using the chemical transport model OsloCTM3, we perform simulations with the CEDS21 emission inventory and compare to previously published results derived with the original CEDS release (Lund et al., 2018; Lund et al., 2019). We also perform simulations with a third recent global inventory, the ECLIPSE version 6b, where emissions are similar in evolution but generally even lower than in CEDS21, especially in the most recent period. We explore~~quantify~~ the differences in ~~between inventories in~~ simulated evolution of global and regional anthropogenic aerosol loads ~~over the 1990-2014 period~~between experiments using the different inventories, comparing optical depth to remote sensing observations, and quantify ~~in~~ the resulting radiative forcing. ~~We also explore the post-2014 aerosol evolutions with CEDS21 and compare trends in simulated aerosol optical depth to remote sensing observations.~~ Our aims are to document the model ability to represent recent observed aerosol trends and to quantify the implications of differences in inventories available for the community on downstream diagnosed quantities critical for assessing the air quality and climate implications of anthropogenic aerosol.

2 Methods

Atmospheric concentrations of aerosols are simulated with the global chemical transport model OsloCTM3 (Lund et al., 2018; Søvde et al., 2012). The model is driven by meteorological data from the European Center for Medium Range Weather Forecast (ECMWF) OpenIFS model updated every 3 hours and is run in a 2.25°x2.25° horizontal resolution, with 60 vertical levels (the uppermost centered

at 0.1 hPa). OsloCTM3 treats tropospheric and stratospheric chemistry, as well as modules for carbonaceous, secondary organic, sulfate, ammonium-nitrate, sea salt and dust aerosols. Aerosols are scavenged by convective and large-scale rain (ice and liquid phase), with rainfall calculated from ECMWF data for convective activity, cloud fraction, and rainfall. Dry deposition applies prescribed deposition velocities for different land cover types. For further details we refer to Lund et al. (2018) and Søvde et al. (2012).

The aerosol optical depth (AOD) and instantaneous top-of-atmosphere radiative forcing due to aerosol-radiation interactions (RFari) is calculated offline using a multi-stream model with the discrete ordinate method DISORT (Myhre et al., 2013; Stamnes et al., 1988). The same radiative transfer model is also used to estimate the radiative forcing of aerosol-cloud interactions (RFaci) (earlier denoted the cloud albedo effect or Twomey effect). To account for the change in cloud droplet concentration resulting from anthropogenic aerosols, which alter the cloud effective radius and thus the optical properties of the clouds, the approach from Quaas et al. (2006), is used. Briefly, this approach is based on a statistical relationship between cloud droplet number concentrations and fine-mode AOD derived from satellite data from the MODerate Resolution Imaging Spectroradiometer (MODIS).

Modeled AOD is compared with retrievals from the MODIS instrument on the Aqua satellite, which is available for the period 2003-2020 (MOD08, 2018). We use the combined Dark Target and Deep Blue AOD at 550nm, release MOD08_M3_V6.1, downloaded from the NASA Giovanni interface. MODIS-Terra AOD is also available for the same period and, for most years, is around 10% lower than MODIS-Aqua on global average. However, based on previous evaluation of the MODIS AOD and a reported drift in the Terra data (Levy et al., 2010; Sherman et al., 2017), we chose to use MODIS-Aqua for the model comparison in the current study. ~~We also compare modeled AOD with ground-based measurements from the AERONET (AErosol RObotic NETwork) (Holben et al., 1998) Version 3 Level 2.0 retrievals at 500 nm. The comparison uses all available data from all months and stations for a given year, with modeled AOD linearly interpolated to the latitude and longitude of each station.~~ Temporal trends in simulated and observed AOD are estimated on global-mean and grid point basis by linear least square fitting and defined as statistically significant (from no trend) when the linear Pearsons correlation coefficient is significant at the 0.05 level. To minimize the influence of individual years, e.g. with higher biomass burning influence, we calculate a set of trends with one and one year removed from the sample and then take the average of this set of coefficients. Interannual variability is estimated on a grid point basis as the standard deviation of the residual when subtracting a 10-year boxcar average (with mirrored data around the end points). We also compare modeled AOD with ground-based measurements from the AERONET (AErosol RObotic NETwork) (Holben et al., 1998) Version 3 Level 2.0 retrievals at 500 nm. The comparison uses all available data from all months and stations for a given year, with modeled AOD linearly interpolated to the latitude and longitude of each station.

Five different time series of simulated aerosol distributions covering the 1990-2019 period are included in this analysis, using three different emission inventories and either fixed or actual (i.e. corresponding to the emission year) meteorology. The fixed meteorology runs forms the basis for investigating differences in simulated anthropogenic aerosol and corresponding RF, while the latter is used in the comparison with observed AOD. Table 1 provides a summary of the experiments.

Two sets of ~~time slice~~fixed meteorology simulations are performed using anthropogenic emissions from ~~the~~ CEDS version 2021 (O'Rourke et al., 2021) (hereafter *"CEDS21"*) and ECLIPSEv6b baseline (hereafter *"ECLv6"*) inventories. The ECLv6 emissions are developed with the Greenhouse Gas - Air

Pollution Interactions and Synergies (GAINS) model (Amann et al., 2011). Version 6b (IIASA, 2022) consists of gridded aerosol and reactive gas emissions in 5-year intervals over the period 1990-2015, as well as emissions for 2008, 2009, 2014 and 2016. The Community Emission Data System (CEDS) inventory provides a gridded inventory of anthropogenic greenhouse gas, reactive gases and aerosols since 1750 (Hoesly et al., 2018). In the first release, the most recent year was 2014, while the 2021 release covers the period until 2019. Simulations ~~with OsloCTM3~~ are performed for 1990, 1995, 2000, 2005, 2010, 2014 and 2016 emissions, as well as years 2018 and 2019 for CEDS21. Results from the current study are compared with previously published results from simulations over 1990 to 2014 performed with the first release of the CEDS emissions (hereafter *"CEDS"*) (Lund et al., 2018) and three of the SSP scenarios (SSP1-1.9, SSP2-4.5, and SSP3-7.0) from 2015 to 2100 (here we use data for 2020 and 2030) (Lund et al., 2019). These three scenarios broadly span the range of aerosol and precursor emissions projected in the SSPs. Keeping in line with the experimental design in Lund et al. (2018), we use year 2010 meteorological data and each simulation is run for one year, with 6 months spin-up. All three time series ~~In all simulations,~~uses biomass burning emissions from van Marle et al. (2017) ~~are used for the~~from 1990 to 2014 ~~period,~~ and ~~with~~ Global Fire Emissions Database version 4 (GFED4, Randerson et al. (2017)) thereafter. We note that van Marle et al. (2017) emissions are also based on GFED. Other natural emissions (dust and sea salt aerosols, precursor gases from the ocean, soil, and vegetation) are fixed at the year 2010 levels.

For the comparison with MODIS data, ~~Additionally, w~~we use ~~output from~~ a timeseries of OsloCTM3 simulations with CEDS emissions and actual ~~actual, running~~ meteorology covering the period 1990-2017 (the last three years uses Shared Socioeconomic Pathways (SSP) 2-4.5 emissions (Fricko et al., 2017) linearly interpolated between 2015 and 2020) (hereafter *"CEDSmet"*). These simulations were ~~Originally~~originally performed for the phase III of the Aerocom project (e.g. Gliß et al., 2021). For the present study, we also produce an updated version covering the 2001-2017 period using CEDS version 2021 emissions (hereafter *"CEDS21met"*)~~,~~. While differences in emissions exist also in the years prior, we restrict the use of resources by only going back to the start of the MODIS record, covering the period when the ~~this time series allows an assessment of the role of meteorology in the simulated aerosol trends. Finally, we produce an updated version of this timeseries using the 2021 release of the CEDS emissions for the 2001-2017 period (i.e. when the~~ differences are most pronounced~~) (hereafter "CEDS21met").~~. In these simulations, the other natural aerosol emissions also vary following the meteorological year. ~~A summary of the experiments is provided in Table S1.~~

~~Figure 1 shows global, total emissions of SO_2, BC, OC and NOx over the 1990-2019 period in the three inventories used here. The differences are particularly pronounced after 2005. Both ECLv6 and CEDS21 show substantially lower emissions of all species during this period, relative to CEDS. The largest differences are for BC and OC, where CEDS21 is 20-30% lower than CEDS in 2014. For SO_2 and NOx, the corresponding number is approx. 10%. ECLv6 is generally lower than both CEDS inventories, particularly for SO_2, where ECLv6 is 30% lower than CEDS. While not used in this study, we also note that similar differences have also been found between CEDS and two other recent global inventories, the Emissions Database for Global Atmospheric Research (EDGAR) version 5 (Crippa et al., 2020) and Hemispheric Transport of Air Pollution (HTAP) version 3 (Crippa et al., 2022). Important geographical distinctions underlie these global differences, as demonstrated for SO_2 emissions in 2014 in Fig. 1~~(Gómez-Sanabria et al., 2022; e.g.Kanaya et al., 2020); Wiedinmyer et al. (2014); Zheng et al. (2018)~~,~~ ~~where lower emissions in ECLv6 and CEDS21 are primarily found in China, India, and the Arabian Peninsula. For many regions and species, differences exist also prior to 2014 (Fig. S1). For instance, CEDS21 has the highest BC emissions in China of the three inventories until year 2000, while ECLv6 BC emissions are higher than CEDS21 in both India and Africa South of the Sahara. In India, CEDS~~

~~and CEDS21 show increasing SO_2 emissions while in ECLv6 these appear to be leveling off during 2014-2016. Aside from East and South Asia, the overall temporal evolution is generally similar in the main source regions across inventories, although magnitudes differ.~~

~~Figure 1 shows global, total emissions of SO_2, BC, OC and NOx over the 1990-2019 period in the three inventories used here. The differences are particularly pronounced after 2005. Both ECLv6 and CEDS21 show substantially lower emissions of all species during this period, relative to CEDS. The largest differences are for BC and OC, where CEDS21 is 20-30% lower than CEDS in 2014. For SO_2 and NOx, the corresponding number is approx. 10%. ECLv6 is generally lower than both CEDS inventories, particularly for SO_2, where ECLv6 is 30% lower than CEDS. While not used in this study, we also note that similar differences have also been found between CEDS and two other recent global inventories, the Emissions Database for Global Atmospheric Research (EDGAR) version 5 (Crippa et al., 2020) and Hemispheric Transport of Air Pollution (HTAP) version 3 (Crippa et al., 2022). Important geographical distinctions underlie these global differences, as demonstrated for SO_2 emissions in 2014 in Fig. 1, where lower emissions in ECLv6 and CEDS21 are primarily found in China, India, and the Arabian Peninsula. For many regions and species, differences exist also prior to 2014 (Fig. S1). For instance, CEDS21 has the highest BC emissions in China of the three inventories until year 2000, while ECLv6 BC emissions are higher than CEDS21 in both India and Africa South of the Sahara. In India, CEDS and CEDS21 show increasing SO_2 emissions while in ECLv6 these appear to be leveling off during 2014-2016. Aside from East and South Asia, the overall temporal evolution is generally similar in the main source regions across inventories, although magnitudes differ.~~

3 Results and discussion

Here we first document the differences in simulated global and regional ~~and trends in~~ aerosol abundances ~~distributions~~ and trends arising from the spread between emission inventories~~simulated with the three different emission inventories~~. We then investigate how AOD diagnosed from experiments using old and new emission estimates compare with observed AOD. ~~, discussing burdens of individual species before focusing on total AOD. We then~~ Finally, we present updated estimates of radiative forcing relative to 1990. ~~Finally, we compare the simulated global and regional AOD with observations over the period.~~

3.1 Influence of emission inventory differences on simulated aerosol distributions~~Aerosol burdens~~

Figure 1 shows global, total emissions of SO_2, BC, OC, NOx, ammonium (NH_3) and non-methane volatile organic compound (NMVOC) over the 1990-2019 period in the inventories used here. The differences are particularly pronounced after 2005. Both ECLv6 and CEDS21 show substantially lower emissions of most species during this period, relative to CEDS. In 2014, the largest differences between CEDS21 and CEDS are in BC and OC emissions, where CEDS21 is 20-30% lower. For SO_2, NOx, and NMVOC, the corresponding number is approximately 10%. ECLv6 is generally lower than both CEDS inventories, particularly for SO_2 and NMVOC, by about 30%. While not used in this study, we also note that similar differences have also been found between CEDS and two other recent global inventories, the Emissions Database for Global Atmospheric Research (EDGAR) version 5 (Crippa et al., 2020) and Hemispheric Transport of Air Pollution (HTAP) version 3 (Crippa et al., 2022).

Important geographical distinctions underlie these global differences, as demonstrated in Fig. S1 for selected main source regions. While a comprehensive investigation of causes for the inventory differences is beyond the scope of the present study, and can be difficult due to the number of underlying assumptions, input data, and revisions, we discuss some key features here. All three inventories rely on the energy statistical data from International Energy Agency (IEA), however, there are differences in assumptions about emission rates, implementation of policies, and data on non-energy sources. The ECLv6 estimates include explicit representation of air quality policies and their implementation efficiency drawing on national information and, if not available, extrapolation of trends considering capacity replacement (e.g., new vehicles, newly build power plant capacity) and emission performance of these new technologies. This led to, among other things, estimated faster decline of SO_2 and NOx emissions from power and industry (in turn in total emissions) in China over recent years than in CEDS (Fig. S1a,d). This decline has been also confirmed in Zheng et al. (2018). CEDS21 made a correction to CEDS, mirroring the estimates in the GAINS model for ECLv6. In South Asia, dominated by India, ECLv6 and CEDS21 show a similar difference to CEDS emissions of SO_2 and NOx, representing use of updated emission characteristics for coal power plants. India has had a slower economic growth and less heavy industry than China. While some policies aimed at controlling NOx from transport has been introduced, the limited polices in the power and industry sector have resulted in increasing Indian SO_2 and NOx emissions, but the growth has been slower than that in China in the 2000's. For BC and OC (Fig. S1b,c), the three inventories show largest differences for East Asia, mainly China, owing to differences in estimates of emissions from coal use in industry, with ECLv6 applying the lowest emission factors, and from open burning of municipal waste. For the latter category, CEDS has originally relied on the rather high estimates of waste generation and share burned (using Wiedinmyer et al. (2014)), while ECLv6 used independently estimated generation rates (Gómez-Sanabria et al., 2022). The declining BC trends in East Asia, as shown in ECLv6 and CEDS21, have been supported by measurements (e.g. Kanaya et al., 2020). Estimates for some species, e.g., NH_3, are often based on very similar sources of information as, apart from in Europe and North America, these have received less attention from policy making and measurement (emissions) community. Consequently, estimates are similar across all inventories at the aggregated regional level (Fig. S1e). Aside from East and South Asia, the overall temporal evolution is generally similar in the main source regions across inventories, although magnitudes can differ.

3.1.1 Global and regional aerosol burdens in 2014

The differences between inventories are substantial enough to influence simulated aerosol burdens (i.e. column integrated aerosol mass, in mg m^{-2}) at the global mean level. For 2014, i.e. the most recent common year for all three emission inventories, we estimate 4% and ~~6~~8% lower global mean burdens of total BC when ~~ith~~ using CEDS21 and ECLv6 (~~increasing to~~ 6% and 11% if ~~when~~ considering only aerosols only from fossil fuel and biofuel combustion~~emissions~~), respectively, compared to CEDS (~~see~~ Table S1~~2 for absolute numbers)~~). For primary organic aerosol (POA), the corresponding numbers are 11% and 1~~4~~3% (30% and 40%), while global mean total sulfate burden is 8% and 15% lower with CEDS21 and ECLv6. Smaller reductions on the order of 3-4% are also seen in the global mean ~~secondary organic aerosol (~~SOA~~)~~ burden. Biogenic ~~volatile organic compound (~~ VOC~~)~~ emissions, the main source of SOA, are the same in all simulations. However, the SOA abundance is affected by the lower emissions of ~~differences in~~ anthropogenic VOCs in both CEDS21 and ECLv6 than in CEDS (Fig.1), as well as ~~and b~~by lower ~~changes~~amount of POA ~~in primary organic aerosols~~, which serve as substrates for SOA formation.

For all these aerosol ~~main anthropogenic aerosol s~~species, the ~~absolute~~burden differences are consistently largest over East Asia, followed by South Asia, and larger for ECLv6 than for CEDS21. Figure 2 shows absolute regional mean burden (with corresponding relative changes given in Fig.S3). Regions considered are East Asia (EAS), South Asia (SAS), Sub-Saharan Africa (SAF), North America (NAM), South America (SAM), North Africa and the Middle East (NAF), Europe (EUR), Southeast Asia (SEA), and Russia (RBU) (see also Fig. S2). For EAS, the new simulated burden of BC and POA is 30-40% lower, depending on inventory, compared to simulations using CEDS, following 50-60% lower BC and OC emissions. The 40-50% lower SO_2 emissions translate to 20-30% lower regional sulfate burden in our simulations. A similar relationship between emission and burden differences are simulated for SAS, where the burdens of BC, POA, and sulfate are 6%, 27%, and 30% lower, respectively, in experiments with ECLv6 than with CEDS. Lower burdens of sulfate and POA are simulated for all other regions as well, and in particular ~~Averaged over these regions, we find reductions in the year 2014 burdens of BC, POA and sulfate of up to 0.45, 3.5, and 1.9 mg m^{-2}, respectively, when switching from CEDS t~~over NAF with ECLv6. In some regions, like SAM, NAF, and SAF, the new inventories estimate 20-30% lower BC emissions than CEDS, however, due to the lower absolute magnitudes, the simulated burden differences are small compared to other aerosols. We note that regional burdens can be influenced by long-range transport and thus affected by ~~remote emission~~ inventory differences outside the main source region. We also note that we find differences in surface concentrations between simulations that are broadly similar ~~track the results for~~to the burden changes. While beyond the scope of the present study, this may have implications for assessments of air pollution related health impacts.

The only species that is globally more abundant ~~globally~~ in simulations with the two new inventories, is nitrate. ~~However, t~~There is~~are~~ considerable ~~important~~ regional heterogeneity~~differences~~, where the burden is lower compared to the CEDS experiments in South Asia and on the US east coast but higher in the US Midwest, parts of Africa and South America, and, especially, over East Asia (Fig.2~~2~~, Fig.S~~2~~3). While absolute differences are small in many regions compared to other species, ~~T~~the net effect is nevertheless a 15 and 24% higher global mean nitrate burden with CEDS21 and ECLv6, respectively, compared ~~relative~~ to using CEDS emissions. Changes in the atmospheric nitrate distribution results from a complex interplay between differences in emissions of NOx, NH_3,~~ammonia,~~ and SO_2. Studies have also shown that nitrate formation can be influenced by background concentrations of VOCs (e.g. Womack et al., 2019)~~.~~ We find the largest absolute difference in nitrate in ~~For instance, in~~ EAS and SAS, however, of opposite sign. In EAS~~China (and elsewhere), the lower~~ emissions of SO_2 and NOx are both lower in ~~both~~ ECLv6 and CEDS21 than in CEDS, whereas NH_3 emissions are higher (Fig.1, Fig.S1). ~~–~~This results in lower ~~reduces the~~ chemical competition for available sulfate and, in turn, enhanced ~~increases the~~ formation~~production~~ of nitrate aerosol. In SAS, SO_2, NOx, and NH_3 are all lower in the two new inventories than in CEDS, as is the nitrate burden. Differences in concentrations of VOCs in the simulations with different inventories is a further complicating factor. Studies have suggested that nitrate formation can be more sensitive to changes in VOCs than NOx, however, this is highly site specific (Yang et al., 2022). Further delineating the role of individual factors on nitrate differences would require simulations beyond what is available for the current study. The potential for an increasing relative role of nitrate for air pollution and climate in a world with concurrent declines in SO_2 and NOx emissions but little in NH_3 has also been discussed in previous studies (e.g. Bauer et al., 2007; Bellouin et al., 2011; Zhai et al., 2021). ~~-~~However, while more studies have focused on local air pollution impacts of nitrate, and associated mitigation strategies, nitrate is still missing from many global climate models. Moreover, when included, the model diversity in simulated distributions is large (Bian et al., 2017). Our results suggests that uncertainties in emissions and choice of inventory can contribute to spread in simulated nitrate aerosols and confound the comparison of conclusions across modeling studies. Moreover, the complexity of the nitrate response demonstrates that the impact of inventory differences on simulated aerosols cannot be understood from scaling with the changes in individual emissions but require explicit modeling.

To place the range in estimates between simulations with different inventories into more context, we compare the differences in simulated aerosol burdens in 2014 to the difference in burdens over the 5-year period from 2014 to 2019 using CEDS21. ~~Averaged globally, we estimate 3% and 6% lower AOD with CEDS21 and ECLv6, respectively, compared to CEDS in 2014.~~

~~Regionally, even larger difference between the two new inventories and CEDS arise, as shown in Fig. 2 (see Fig. S2 for corresponding percentage changes). For all main anthropogenic aerosol species, the absolute differences are consistently largest over East Asia, followed by South Asia, and larger for ECLv6 than for CEDS21. Averaged over these regions, we find reductions in the year 2014 burdens of BC, POA and sulfate of up to 0.45, 3.5, and 1.9 mg m^{-2}, respectively, when switching from CEDS to ECLv6 (Fig. 2). This constitutes changes of around 30-40% (Fig. S2). For BC and sulfate, burdens are also notably lower over North Africa and the Middle East with ECLv6 compared to both CEDS and CEDS21.~~

~~The only species that is more abundant globally with the two new inventories, is nitrate. However, there are important regional differences, where the burden is lower compared to CEDS in South Asia and on the US east coast but higher in the US Midwest, parts of Africa and South America, and, especially, over East Asia (Fig.2, Fig.S2). The net effect is a 15 and 24% higher global mean nitrate burden with CEDS21 and ECLv6, respectively, relative to CEDS. Changes in the atmospheric nitrate distribution results from a complex interplay between differences in emissions of NOx, ammonia, and SO_2. For instance, in China (and elsewhere), the lower emissions of SO_2 in both ECLv6 and CEDS21 reduces the chemical competition for available sulfate and, in turn, increases the production of nitrate aerosol. The potential for an increasing relative role of nitrate in a world with concurrent declines in SO_2 emissions has also been discussed in previous studies (!!! INVALID CITATION !!! (e.g. Bauer et al., 2007; Bellouin et al., 2011)).~~

~~B~~Both globally and regionally, th~~e~~e spread in burdens between simulations with different inventories and the 2014-2019 burden changes are of~~spread in estimated aerosol load in 2014 between simulations with different inventories is on~~ the same order of magnitude. ~~or larger than the change over the 5-year period from 2014 to 2019 in CEDS21.~~ In other words, at least in this case, the changes resulting from inventory differences are as large as those due to the recent overall change in anthropogenic emissions. ~~We note that regional burdens can be influenced by long-range transport and thus affected by remote emission inventory differences. We also note that we find differences in surface concentrations between simulations that broadly track the results for burden. While beyond the scope of the present study, this may have implications for assessments of air pollution related health impacts.~~

Combined, these burden differences translate to a 3% and 6% lower global, annual mean AOD with CEDS21 and ECLv6, respectively, compared to CEDS in 2014 in our simulations. As expected, the differences are most pronounced over China and India (Fig. S4), where we estimate 20% and 30% lower regional mean AOD in 2014 using the two new emission inventories, respectively, compared to using CEDS. For context, Fig. S4 also shows the interannual variability in AOD from MODIS-Aqua (see Sect. 2): In these regions the differences between inventories are markedly larger than what can be expected from natural year-to-year variations.

3.1.2 Global and regional AOD 1990-2019

~~Regional differences are larger and, as expected, most pronounced over China and India (Fig. 3b). Averaged over each of these regions (indicated by the boxes in Fig.3b), we estimate 20% and 30% lower~~

~~AOD using the two new emission inventories, respectively, in 2014. For context, we also show the interannual variability in AOD from MODIS-Aqua (see Sect. 2): For most of these regions the differences between inventories are markedly larger.~~Next, we take a closer look at differences in the simulated temporal trend, focusing on total AOD. Figure 3 shows the global and regional mean AOD from 1990 to 2019. Also shown is ~~plotted in Fig. 3a is~~ the linear trend from 2005 to 2017 for each of the ~~global timeseries~~timeseries. This period overlaps with the availability of remotely sensed AOD discussed in Sect. 3.1.3, as well as the period with the most pronounced inventory differences. However, as there is a certain extent of inventory differences also prior to 2005, we also provide corresponding linear trends over the full 1990-2017 period in Table S2.

The simulated AOD is consistently lower when

~~**3.2 Aerosol optical depth**~~

~~The differences between inventories are also directly reflected in the simulated total AOD. Over the whole period considered, global mean AOD is highest in simulations with the first release of the CEDS emissions, followed by~~ using CEDS21 and ~~then~~ ECLv6 emissions compared to CEDS~~,~~ over the full period studied, with increasing divergence over time, especially after 2005 ~~(Fig. 3a)~~. ~~Averaged globally, we estimate 3% and 6% lower AOD with CEDS21 and ECLv6, respectively, compared to CEDS in 2014. Regional differences are larger and, as expected, most pronounced over China and India (Fig. 3b). Averaged over each of these regions (indicated by the boxes in Fig.3b), we estimate 20% and 30% lower AOD using the two new emission inventories, respectively, in 2014. For context, we also show the interannual variability in AOD from MODIS-Aqua (see Sect. 2): For most of these regions the differences between inventories are markedly larger.~~

~~Also plotted in Fig. 3a is the linear trend from 2005 to 2017 for each of the global timeseries.~~ We estimate a significant (at the 0.05 level - see Sect. 2) negative linear trend in global mean AOD of -0.005 and -0.006 per decade in simulations with ~~that anthropogenic emission changes in the~~ CEDS21 and ECLv6 ~~inventories have resulted in a significant (at the 0.05 level - see Sect. 2) negative linear trend in global mean AOD of -0.005 and -0.006 per decade~~, respectively. This trend strengthens when extended to 2019 based on simulations with ~~in~~ CEDS21. A negative global trend is also found when using the first CEDS release, however, it is smaller and not significant over the period 2005-2014. Extending the timeseries to 2017 by assuming that emissions follow SSP2-4.5 after 2014 (see Sect. 2)~~dashed orange line)~~, as in Fig. 3, the negative trends strengthens and switches to significant as per our definition, but it remains weaker ~~smaller~~ than for the other two inventories ~~(at -0.003 per decade)~~. Considering the full period, we estimate a significant negative trend in simulations with CEDS21 and ECLv6, but no trend when using CEDS (Table S2). This long-term decline in total AOD is primarily driven by the decline in sulfate AOD, following the emission decline after introduction of air quality policies, first in the US and Europe, then in China, and the collapse of the Soviet Union (e.g. Aas et al., 2019). Over the full period, we simulate increasing trends in BC and nitrate AOD, significant at the 0.05 level, with all three inventories (not shown), however, their contributions to total AOD are much smaller than that of sulfate. Robust evidence of a declining influence by aerosols on climate since 1990 was recently found from observables (Quaas et al., 2022). Our model simulations capture this overall trend, and the findings reinforce the role of changes in anthropogenic emission, particularly since 2005. Furthermore, we suggest that if using the original CEDS emissions, models may have failed to capture this trend. We note that biomass burning emissions also change over time in our simulations, but we do not find any significant trend in biomass aerosols (BC and POA) AOD on the global mean scale over this period. We do note that years of high biomass burning activity, such as 2019 where GFED4 emissions are 25% higher than in 2018, can lead to marked jumps in simulated AOD. We have limited possible influence of such years on the linear trend calculated (see Sect. 2). ~~t despite the negative long-term trend and continued decrease in anthropogenic emissions, CEDS21 AOD is up in 2019 compared to 2018. We attribute this primarily to the high 2019 biomass burning emissions in GFEDv4, more than 25% higher than in 2018.~~

Regionally, we simulate significant declining trends in ~~all three emission inventories result in a significant decline in~~ AOD over 2005-2017 for ~~over~~ EUR~~the Eastern US~~ and ~~, Europe, and~~ NAM, with this ~~parts of Russia and Eurasia over the 2005-2017 period in our simulations (Fig. 3c).~~trend extending back to 1990 (Table S2), as expected. This is also consistent with surface observations both AOD and atmospheric sulfur and in agreement with other models (Mortier et al., 2020; Aas et al., 2019), and we capture the decline regardless of which emission inventory is used. In both regions, and across simulations with all three scenarios, we find a decline in the AOD of BC, OA, and sulfate, but an increasing trend in nitrate AOD. Over RBU, we also simulate a decline a significant decline in area average AOD over the full 1990-2017 period, but a flatter evolution when considering only 2005-2017. However, the results are similar with all three scenarios also here. In parts of the RBU region, GFED4 shows an increase in emissions over the latter period, resulting in a positive trend in the AOD of biomass aerosols from 2005. On the African continent, we simulate negative, albeit weak, trend in AOD over the 2005-2017 period for SAF. In contrast, the trend over the full period is positive. Anthropogenic emissions in SAF have increased (Fig. S1), although less steeply than in Asia, and we find significant increases in the AOD of all the anthropogenic species with all inventories from 1990 to 2017. However, from 2005 onwards, there has been a decreasing trend in GFED4 emissions, following a reduction in the burnt area of savannas (Wu et al., 2021). Biomass burning aerosols contribute relatively more to total AOD here, than in the northern hemisphere regions and hence impose a stronger effect on the area average trend. A similar pattern is seen for SAM, while for SEA, another biomass burning influenced region, we find less clear trends. While diagnosed trends in total AOD in these regions are mostly of similar sign across simulations with the three inventories, we find that the trend in sulfate AOD diverges between model runs using CEDS or CEDS21 (positive trend) and ECLv6 (negative trend) in SAF and NAF, pointing to a need to better understand the drivers of emission changes in these regions and homogenize between inventories. As expected, the key differences between simulations with different inventories arise over Asia. Simulations with ~~There is also a marked negative trend over South America, as well as a weaker decline over Equatorial Africa. In contrast, increases in simulated AOD are seen over Eastern Siberia. A positive, but weaker and not significant at the 0.05 level, trend is also seen over Canada. This is presumably due to higher biomass burning activity, which is supported by a significant increasing trend in annual biomass burning carbon emissions in GFEDv4 in the boreal North America and eastern Eurasia regions over the same period (not shown). There is also a decline in GFEDv4 carbon emissions in South America and Africa south of the Sahara, suggesting that biomass burning is also a key driver of the simulated AOD trends there. While the three inventories largely agree in all of above regions, the key differences arise, as expected, when looking at Asia. B~~both CEDS21 and ECLv6 show a significant decreasing trend in total AOD over EAS between 2005 and 2017~~China~~. While ~~A~~a decline is found ~~also present in the simulations with~~using CEDS, it ~~— when extending the time series to 2017 using SSP245 emissions — but~~ is much weaker and not significant. Moreover, differences between inventories affect the sign of the simulated trend when considering the full period, owing primarily to the spread in estimated sulfate AOD. For SAS, we simulate a consistent positive trend, but ranging from 0.01 per decade with ECLv6 to 0.03 per decade with CEDS, with increasing divergence in AOD over time. Similar magnitude differences between the sets of experiments exist for the AOD of all anthropogenic aerosol in this region. ~~Real world emissions have hence likely tracked well below the SSP245 projections in the region. While all three inventories show a significant positive trend in AOD over India, this is strongest in CEDS. Regional trends and differences will be further discussed in Sect. 3.4, including a comparison with observations.~~

~~3.3 Radiative forcing of anthropogenic aerosol since 1990~~

Figure 4a shows the RFari, RFaci, and net aerosol radiative forcing (RFnet, RFari plus RFaci) relative to 1990 for the three sets of experiments. The net RF of changes in anthropogenic (and biomass burning) aerosol is positive since 1990, except for 1995 and 2005, where a small negative forcing is estimated. As shown in Fig. 1, all inventories show an increase in anthropogenic SO_2 emissions in 2005 compared to the years before, and both these years have relatively high biomass burning emissions in these years. This positive global mean RF is determined by the balance between a positive forcing over the northern extratropics, predominantly due to aerosol-radiation interactions, and a negative forcing over Asia and parts of South America and Africa (Fig. S3).

In 2014, we estimate a global mean RFnet of 0.03 W m^{-2} for CEDS, 0.08 W m^{-2} for CEDS21, and 0.12 W m^{-2} for ECLv6 relative to 1990, of which the RFari constitutes 0.07 W m^{-2}, 0.09 W m^{-2} and 0.10 W m^{-2}. Our CEDS RFari estimate is similar to the multi-model mean RFari of 0.05 W m^{-2} derived for the 1990-2015 period using ECLIPSE version 5 emissions by Myhre et al. (2017). The same study estimated a model mean RFnet of 0.1 W m^{-2}, but with a significant intermodel spread, from close to zero to more than 0.2 W m^{-2}. This spread is larger than the difference between estimates with different inventories in the present analysis. Nevertheless, the differences in emissions between CEDS and CEDS21 (ECLv6) translates to a factor 3 (5) stronger RFnet in our calculations. These differences arise primarily from the weaker forcing over East Asia and, for ECLv6, also over South Asia and South and Central America, compared to CEDS (Figure 4b). In contrast, all three inventories give similar RF over the 1990-2014 period in North America, Europe, and Eurasia and show the effect of the southeastward shift in emissions over the past decades. A negative forcing is seen over China during this period with all three inventories; however, this is markedly weaker in CEDS21 and ECLv6 (Fig. S3).

Figure 4c shows the RFnet in 2019 relative to 2014, i.e. the five most recent years provided by CEDS21. In contrast to the 1990-2014 period (Fig. S3), a net positive forcing is estimated over China, in line with the decline in SO_2 emissions. Over India, the forcing has remained negative, although weaker than during the preceding period. Over Europe and western Russia, the bulk of the emission decline, and hence forcing, was already realized until 2014, with only relatively weaker RF seen until 2019. On global average, RFnet is estimated to be 0.10 W m^{-2} in 2019 relative to 1990 for CEDS21 emissions (small reduction from 0.13 W m^{-2} in 2018 likely due to stronger biomass burning emissions in 2019) (Fig. 4a).

In the first CEDS release, the most recent historical year was 2014. Using a selection of the SSP scenarios, Lund et al. (2019) quantified the projected aerosol-induced RF. The orange hatched bars in Fig. 4 show the range in RFnet in 2020 and 2030 (relative to 1990) estimated with SSP1-1.9, SSP2-4.5 and SSP3-7.0 in that study. The RFnet in 2019 estimated with CEDS21 is close to the lower end of the bar, i.e. the RFnet projected under SSP3-7.0. However, prior to this higher biomass burning year, there are indications that the RFnet from simulations with CEDS21 tracked closer to SSP2-4.5 or an even lower emission pathway.

The dipole pattern of aerosol changes and resulting RF over India versus China was first highlighted by Samset et al. (2019). Using emissions from CEDS and SSP1-1.9, SSP2-4.5 and SSP3-7.0, combined with a radiative kernel approach, that study estimated a range of 2014-2030 aerosol (SO_2 and BC) RF of -1.0 W m^{-2} (SSP1-1.9) to 0.82 W m^{-2} (SSP2-4.5) over India, and 0.06 W m^{-2} (SSP2-4.5) to 1.10 W m^{-2} (SSP3-7.0) over China. Part of this range can be attributed to poor knowledge of current, and hence also future, regional emissions (Samset et al. 2019). In the present study, we estimate regionally averaged RFnet in 2019 relative to 2014 of -0.09 W m^{-2} and 0.22 W m^{-2} over India and China, respectively. For China, this recent RFnet is about 20% of the previously estimated difference between high and low future aerosol emission scenarios in 2030 (SSP2-4.5 and SSP3-7.0). Uncertainties in the amount of recent emission reductions can therefore markedly affect assessments of projected near-tern aerosol-induced climate impacts, as they depend on a well constrained starting point.

3.1.34 Comparison with observed AODaerosol trends

To explore We have demonstrated that the differences between recent global inventories translates to notable differences in global and regional anthropogenic aerosol distributions, trends, and radiative forcing. To assess whether the model captures observed global and regional trends better with the CEDS21 emissions than with CEDS, we compare simulated AOD to MODIS-Aqua retrievals and ground-based AERONET measurement. For this evaluation, we also use simulations where the model is driven by meteorology for the respective years, referred to as CEDSmet and CEDS21met, are used (see Sect. 2), for more realistic comparison with the observations. Using both these, we also estimate negative linear trends in simulated global mean AOD from 2005 to 2017, strengthening from -0.001 per decade in CEDSmet to -0.003 per decade in CEDS21met. These are, however, weaker than the trends derived from the fixed meteorology simulations in Sect. 3.1.2 (Fig. 3) and not significant at the 0.05 level, demonstrating the notable influence of variability in meteorology and natural aerosols, masking trends due to changes in anthropogenic emissions. This influence is particularly visible for the area averaged AOD for SAF and NAF, where the diagnosed trend is positive but non-significant in these simulations, in contrast to the negative trend found in simulations with fixed meteorology above. The negative trend over SAM is also not significant at the at the 0.05 level in these runs. For other focus regions, results are similar between fixed and actual meteorology runs and significant trends arise over the natural variability.

Figure 4a shows the annual, global mean simulated AOD from 1990 to 2017 and the MODIS-Aqua AOD from 2003 to 2019. Dashed lines show the linear 2005-2017 trends. Figures 4b-d show the spatially explicit trends. Figure 5a shows the annual, global mean simulated AOD from 1990 to 2017 and the MODIS-Aqua AOD from 2003 to 2019. Dashed lines show the linear 2005-2017 trends. Figures 5b-d show the spatially explicit trends.

We first note that The the magnitude of simulated global mean AOD is lower than that derived from the MODIS-Aqua, by around 20%. However, the overall geographical pattern of the observed AOD is captured by the model (Fig. S54). Furthermore, the AOD simulated by the OsloCTM3 is within, although in the lower range, of the spread in AOD between the CMIP and AeroCom models (Vogel et al., 2022). As also shown by Vogel et al. (2022), there can be a notable spread also in AOD derived from different satellite products. They found a 13% standard deviation range in global mean AOD between eight satellite products, ; wherewith MODIS retrievals comes out in the upper end. Furthermore, although again the lower range, Tthe OsloCTM3 AOD falls is within the full range standard deviation range ofof the satellite- derived annual mean AOD found in that study. Overall, this suggests a reasonable OsloCTM3 performance in terms of magnitude and distribution.

In terms of temporal evolution, we estimate weakly negative linear trends in simulated global mean AOD from 2005 to 2017 with both CEDS and CEDS21, albeit not significant at the 0.05 level. Using the original release of the CEDS emissions with the SSP2-4.5 extension (i.e. CEDSmet), we calculate a trend in global mean AOD of -0.001 per decade. With CEDS21 emissions, this strengthens to -0.003 per decade. These are weaker than the trends associated with anthropogenic emission changes derived from the fixed meteorology simulations in Sect. 3.1 (-0.003 and -0.005 per decade with CEDS and CEDS21, respectively) and not significant, demonstrating the influence of variability in meteorology and natural aerosols. Consistent evidence of a declining influence of anthropogenic aerosols on climate has also been found for a range of observed variables (Quaas et al., 2022). Consistent evidence of a declining influence of anthropogenic aerosols on climate has also been found for a range of observed variables (Quaas et al., 2022).

In contrast, MODIS-Aqua data indicatessuggests a very weak positive linear trend of 0.001 per decade in global mean AOD over the 2005-2017 period (, further strengthening to 0.004 per decade when extending the data to considering the full time series of available observations (2003 2019). We do not, however, find this trend to be significant at the 0.05 level. MODIS data is influenced by This could in

part be due to influence from the substantial year-to-year variability, in particular seen aafter 2010, which was also pointed out by Vogel et al. (2022). Regions of significant positive observed AOD trend include parts of the ocean in the southern hemisphere A positive global AOD trend was also found in ground based observations by Mortier et al. (2020). This positive observed trend is driven by an increase in AOD over oceans, associated with sea salt aerosol, as well as over boreal regions in the northern high latitudes, associated with biomass burning aerosol (Fig. 54b). Here, sea salt aerosols could be causing the increase. However, Quaas et al. (2022) recently showed that this positive trend is not clear in Multi-angle Imaging SpectroRadiometer (MISR) data. We do not, however, find this trend to be significant at the 0.05 level. This could in part be due to influence from the substantial year-to-year variability seen after 2010, which was also pointed out by Vogel et al. (2022). While we are primarily focused on the anthropogenically-influenced regions in the present analysis, we briefly note that the model does not fully capture the magnitude of the trends over high latitude boreal biomass burning regions, nor over the sSouthern hemisphere oceanic regions is also not captured by the model (Fig. 45c-d). While studies to date show a wide spread in simulated response of sea spray aerosol to changing climate, recent studies have suggested increases both at the global (Struthers et al., 2013) and, even more strongly, at the regional scale (Korhonen et al., 2010). Moreover, other factors than wind speed are proposed to be possible drivers of a climate feedback on sea salt aerosol (e.g. Paulot et al., 2020, and references therein). Better understanding of changing natural aerosols in the OsloCTM3 and reasons for the discrepancies compared to observations require further, dedicated studies.We also simulate weaker trends in the boreal regions of North America and Russia, contributing to the model-observation difference.

Over the main anthropogenic emission sources regions, Regionally, there are significant observed declines in AOD over East Asia, eastern US, and parts of Europe (Fig. 45b). These trends have been confirmed by both ground based and remote sensing observations of AOD and other variables (Gui et al., 2021; Moseid et al., 2020; Paulot et al., 2018; Quaas et al., 2022). For NAM and EUR, we calculate an area average negative observed trend of -0.006 and -0.009, respectively, from MODIS-Aqua. This is of the same sign but weaker than the trend simulated with both emission inventories. For the latter, this contrast findings by Mortier et al. (2020), where models in general were found to underestimate the observed decrease in AOD seen in surface observations. Over EAS, where the influence of inventory differences is most pronounced, a significant negative observed trend of -0.044 per decade is calculated. This is in very close agreement with the -0.40 per decade AOD trend simulated with the CEDS21, while simulations with CEDS do not show a significant trend. Hence, the model is clearly able to better represent observed trends with the updated inventory. This is further confirmed in Fig. 5, where we show five-year average deviations from the period 2003-2017 in both MODIS-Aqua and simulated AOD. Using CEDS21 results in marked improvements compared to observed AOD trends over China, both for the first and most recent full 5-year periods. However, the opposite tendency is found for AOD over SAS. Here we estimate and observed significant positive trend of 0.04 per decade. The diagnosed trends are also positive in simulations using both inventories, but somewhat weaker, especially when switching from CEDS to CEDS21 (and even more so when using EClv6 emissions - Fig.3). Figure 5 suggests that this discrepancy arises in the more recent decade. Furthermore, inventories and simulated AOD suggest a leveling off in the increase in recent years, which is not seen from MODIS-Aqua. Whether this is due to inaccurate representation of the evolution of anthropogenic emissions in the inventories or could be influenced by poor model representation of other aerosols such as dust from agricultural soils and urban areas (e.g. construction, non-exhaust transport emissions), is however not clear from this analysis. We note that the model underestimates the magnitude of AOD observed by MODIS-Aqua in both EAS and SAS. To the extent that the MODIS is accurate, this could support the latter. This type of dust is suggested to give an important contribution to the particulate matter load (e.g. Chen et al., 2019; Xia et al., 2022), but are stilling missing from many global models. Other contributing factors include the representation of processes related to aerosol transport and scavenging. Finally, A negative trend is also seen over South America; however, this is not significantly different from zero over this period. A significant positive trend is seen over India. The trends over North America, Europe,

and Asia are consistent with the concurrent changes in anthropogenic emissions and have been seen in both ground based and remote observations of both AOD and other variables (Gui et al., 2021; Moseid et al., 2020; Paulot et al., 2018; Quaas et al., 2022). The trends in AOD simulated with the OsloCTM3 show the same sign as MODIS-Aqua in most regions, for both emission inventories (Fig. 5c-d). As expected from results in preceding sections, the main differences, between CEDSmet and MODIS-Aqua, as well as between model results, arise over Asia. We therefore take a closer look at the evolution of AOD in this region (Fig. 6). Both MODIS-Aqua and the OsloCTM3 show an increase in AOD over India from 2008, although modeled changes are weaker in magnitude. As indicated by preceding sections, using CEDS21 results in marked improvements compared to observed AOD trends over China, both for the first and last full 5-year periods. A continuation of the dipole pattern of increases and decreases over India and China is evident from the observations for the 2018-2020 period (noting that the COVID-19 pandemic resulted in significant temporary impacts on emissions in 2020). In the case of India, this increase suggests that the leveling off in anthropogenic emissions in the inventories (Fig. S1) may not be representative of the observed evolution. However, we note that natural emissions, as well as long-range transport, may factor into the observed trend as well, complicating the comparison. Wwe also note that the 5-year deviations in Fig. 5 show exhibit quite some variability over the Middle East, with both positive and negative deviations from the baseline period. While anthropogenic emissions in this region increase steadily over the period (by 13-40% depending on species) in the inventories used in the present study, the strong influence from dust emissions in this region likely dominates the contributes to the temporal variability.

A previous OsloCTM3 study by Lund et al. (2018) found an improved agreement between year 2010 ground-based AERONET observations and model output, including over Asia, when switching from CMIP5 and ECLIPSEv5 emissions to CEDS, the latter having higher emissions. This seemingly contradicts expectations following the now-known biases in this first release of CEDS. Here we repeat the comparison with AERONET measurements, but for year 2014. Resulting scatter density plots are given in Fig. S6the SI.

On global average, the model underestimates observed AOD, consistent with the comparison against MODIS-Aqua and Lund et al. (2018). The normalized mean bias (NMB) compared to AERONET ranges from -212 to -29% in the simulations with fixed and actual meteorology (Fig. S5). This underestimation is somewhat larger than what was found by Lund et al. (2018), but since the year, number of measurements and stations are different, a direct comparison is difficult. These simulations use 2010 meteorology, however, the difference in meteorology appears to only explain a small part of the bias, as can be seen by comparing scatter density plots for CEDS and CEDSmet and CEDS21 and CEDS21met. Interannual variability may also play a role. We consistently find higher bias NMB and lower correlation when switching from the original CEDS release to CEDS21 and ECLv6. The largest normalized mean bias (NMB) of -29% is found in the simulation using ECLv6 emissions, the lowest of the three inventories, while the smallest NMB is calculated for CEDS (-22%) (Fig. S5). Hence, while the model is better able to represent observed recent aerosol trends over East Asia with newer emission inventories, these results point to other issues that may have been . Specifically, our analysconcealed by too high anthropogenic emissions. Dust and atmospheric processing, as discussed above, are again a possible contributing factors. is indicates that the too high emissions in CEDS may have partly concealed underestimations of other aerosol sources in the model. One possible candidate is dust aerosol from soils in agricultural regions and human activities in urban areas (e.g. construction, non-exhaust transport emissions), which are suggested to give an important contribution to the particulate matter load (e.g. Chen et al., 2019; Xia et al., 2022), but is stilling missing from many global models, including the OsloCTM3.

~~3.3 Radiative forcing of anthropogenic aerosol since 1990~~3.2 Impact of inventory differences on estimated anthropogenic aerosol RF

Finally, we quantify the aerosol-induced RF from the three sets of experiments.

Figure 6~~4~~a shows the RFari, RFaci, and net aerosol radiative forcing (RFnet, RFari plus RFaci) relative to 1990 for the three sets of experiments. The net RF of changes in anthropogenic (and biomass burning) aerosol is positive since 1990, except for 1995 and 2005, where a small negative forcing is estimated. As shown in Fig. 1, global ~~all inventories show an increase in~~ anthropogenic SO_2 emissions show a peak ~~emissions~~ in 2005 ~~compared to the years before,~~ and ~~both these years have~~ the ~~relatively high~~ biomass burning emissions are relatively high~~in these years~~. This positive global mean net RF is determined mainly by the balance between a positive forcing over the northern extratropics, ~~predominantly~~dominated by ~~due to~~ aerosol-radiation interactions, and a negative forcing over Asia and parts of South America and Africa with stronger contributions from aerosol-cloud interactions (Fig. S3~~7~~).

In 2014, we estimate a global mean RFnet of 0.03 W m^{-2} for CEDS, 0.08 W m^{-2} for CEDS21, and 0.12 W m^{-2} for ECLv6 relative to 1990, of which the RFari constitutes 0.07 W m^{-2}, 0.09 W m^{-2} and 0.10 W m^{-2}, respectively. We note that our framework only captures the cloud albedo effect and not radiative effects of any changes in cloud lifetime that may arise through the influence of aerosols (i.e. we calculate RF, not ERF). Our ~~CEDS~~ RFari estimate using CEDS emissions is similar to the multi-model mean RFari of 0.05 W m^{-2} derived for the 1990-2015 period using ECLIPSE version 5 emissions by Myhre et al. (2017). The same study estimated a model mean RFnet of 0.1 W m^{-2}, but with a significant intermodel spread, from close to zero to more than 0.2 W m^{-2}. This spread is larger than the difference between estimates with different inventories in the present analysis. Nevertheless, the differences in emissions between CEDS and CEDS21 (ECLv6) translates to a factor 3 (5) stronger RFnet in our calculations.

Figure 6b shows regional mean RF, including the balance between RFari and RFaci. Following the significant decline in AOD over EUR and NAM, the dominant contributions to positive RF are found here, followed by Russia. There is however little difference between simulations with three inventories. In contrast, the net RF over EAS switches sign from negative in simulations with CEDS to positive when using CEDS21 or ECLv6 due to observed decline in emissions now captured. While negative in all three sets of experiments, the net RF over SAS is 40% (20%) weaker when ECLv6 (CEDS21) emissions are used compared to CEDS. This results from a 50% (20%) lower net area averaged AOD change between 1990 and 2014, compared to simulations with CEDS.

~~These differences arise primarily from the weaker forcing over East Asia and, for ECLv6, also over South Asia and South and Central America, compared to CEDS (Figure 4b). In contrast, all three inventories give similar RF over the 1990-2014 period in North America, Europe, and Eurasia and show the effect of the southeastward shift in emissions over the past decades. A negative forcing is seen over China during this period with all three inventories; however, this is markedly weaker in CEDS21 and ECLv6 (Fig. S3).~~

The CEDS21 inventory extends to 2019, compared to 2014 in CEDS. The global mean net RF over this five-year period is estimated to be 0.10 W m^{-2}, driven primarily by a further positive forcing over China in line with the continued decline in SO_2 emissions following implementation of measures targeting improved air quality. Over India, the forcing in 2019 relative to 2014 remains negative, but weaker than during the preceding period, while over Europe and western Russia, the RF is low suggesting little further recent emission changes (not shown). We note however that this is short period and results should be interpreted with that in mind. ~~Figure 4c shows the RFnet in 2019 relative to 2014, i.e. the five most recent years provided by CEDS21. In contrast to the 1990-2014 period (Fig. S3), a net positive forcing is estimated over China, in line with the decline in SO_2 emissions. Over India, the forcing has remained negative, although weaker than during the preceding period. Over Europe and western Russia, the bulk~~

~~of the emission decline, and hence forcing, was already realized until 2014, with only relatively weaker RF seen until 2019. On global average, RFnet is estimated to be 0.10 W m^{-2} in 2019 relative to 1990 for CEDS21 emissions (small reduction from 0.13 W m^{-2} in 2018 likely due to stronger biomass burning emissions in 2019) (Fig. 4a).~~ Using a selection of the SSP scenarios, Lund et al. (2019) extended simulations from 2014 CEDS emissions and quantified the projected aerosol-induced RF. The orange hatched bars in Fig. 6 show the range in RFnet in 2020 and 2030 (relative to 1990) estimated with SSP1-1.9, SSP2-4.5 and SSP3-7.0 in that study. The RFnet in 2019 estimated with CEDS21 here is close to the lower end of the bar, i.e. the RFnet projected under SSP3-7.0. However, prior to this higher biomass burning year, there are indications that the RFnet from simulations with CEDS21 tracked closer to SSP2-4.5 or an even lower emission pathway.

~~In the first CEDS release, the most recent historical year was 2014. Using a selection of the SSP scenarios, Lund et al. (2019) quantified the projected aerosol-induced RF. The orange hatched bars in Fig. 4 show the range in RFnet in 2020 and 2030 (relative to 1990) estimated with SSP1-1.9, SSP2-4.5 and SSP3-7.0 in that study. The RFnet in 2019 estimated with CEDS21 is close to the lower end of the bar, i.e. the RFnet projected under SSP3-7.0. However, prior to this higher biomass burning year, there are indications that the RFnet from simulations with CEDS21 tracked closer to SSP2-4.5 or an even lower emission pathway.~~

The dipole pattern of aerosol changes, and resulting RF, over India versus China that can be seen continuing in observations and is expected to impose regional climate impacts, was first highlighted by Samset et al. (2019). Using emissions from CEDS and SSP1-1.9, SSP2-4.5 and SSP3-7.0, combined with a radiative kernel approach, that study estimated a range of 2014-2030 aerosol (SO_2 and BC) net RF of -1.0 W m^{-2} (SSP1-1.9) to 0.82 W m^{-2} (SSP2-4.5) over India, and 0.06 W m^{-2} (SSP2-4.5) to 1.10 W m^{-2} (SSP3-7.0) over China. Part of this range can be attributed to poor knowledge of current, and hence also future, regional emissions (Samset et al. 2019). In the present study, we estimate regionally averaged RFnet in 2019 relative to 2014 of -0.09 W m^{-2} and 0.22 W m^{-2} over India and China, respectively. For China, this recent RFnet is about 20% of the previously estimated difference between high and low future aerosol emission scenarios in 2030 (SSP2-4.5 and SSP3-7.0). Missing or incorrectly captured ~~Uncertainties in the amount of recent~~ past emission trends~~reductions~~ can therefore markedly affect assessments of projected near-term~~n~~ aerosol-induced climate impacts, as they depend on a well constrained starting point.

4 Conclusions

We have investigated the impact of differences between recent global emission inventories available for the aerosol and climate modeling community on simulated anthropogenic aerosol abundances, and associated radiative forcing, from 1990 to 2019. Simulations with the chemical transport model OsloCTM3 and the CEDS emission inventory, developed for the sixth cycle of the IPCC, has been~~are~~ compared with corresponding results using two newer inventories: The CEDS 2021 update (CEDS21) and the ECLIPSE version 6b (ECLv6). Our objective was to evaluate the model performance considering revisions to the emissions input data, partly done to correct known regional biases, and to investigate the implications of inventory differences on downstream diagnosed quantities critical for assessing the air quality and climate effects of anthropogenic aerosol.

~~Our main objective was to explore the implications of now known biases in CEDS, specifically the underestimation of the decline in Chinese precursor emissions and an overestimation of Asian and~~

~~African BC and OC emissions. While largely addressed in the updated release, these biases introduce added uncertainty in recently published estimates of the anthropogenic aerosol evolution and effects.~~

We have found that, apart for nitrate, simulations with the CEDS21 (ECLv6) inventory give ~~result in~~ lower global mean aerosol burdens than corresponding runs with CEDS, ranging from 4% (6%) for BC to ~~o 18p~~approx~~.~~. 10% (15%) for sulfate and POA in 2014 (the most recent historical year common for all scenarios). Differences are consistently most pronounced over East Asia, followed by South Asia, where they are on the order of 30-60% depending on species and scenario. Difference in the underlying anthropogenic emissions arise from different assumptions about emission rates, data on non-energy sources, and, importantly, representation of air quality policies and their implementation efficiency. ~~We also note marked differences between CEDS and ECLv6 over North Africa and the Middle East.~~ In our model, the global mean fine mode nitrate burden is 15% (24%) higher with CEDS21 (ECLv6) relative to CEDS, but with regional heterogeneity in sign of the difference. Overall, we estimate 3% (6%) lower total AOD with CEDS21 (ECLv6), respectively, compared to CEDS in 2014. The difference reaches ~~18a~~pprox~~.~~. 20% and 30% over East and South Asia.

Over East Asia, we diagnose a significant negative linear trend in total area averaged AOD from 2005 to 2017 of -0.03 per decade in simulations using the ECLv6 emissions. In contrast, we find no significant trend in corresponding experiments with CEDS. ~~Changes in anthropogenic emissions result in a negative linear trend in global mean AOD over the 2005-2017 period with all three inventories, but increasingly stronger with CEDS21 (ECLv6).~~ Importantly, we find that the model is better able to capture the ~~declining AOD t~~trend observed by MODIS-Aqua ~~over China~~ with both new inventories~~, whereas it is weak and not significant with CEDS~~. In all three sets of simulations, we estimate a significant ~~A~~ positive linear AOD trend ~~is found~~ over South Asia~~India~~. The simulated trend is, however, ~~; however, it is~~ weaker than that derived from ~~in the model than in~~ MODIS-Aqua ~~data~~ and this gap increases when switching from CEDS to the CEDS21 and ECLv6 inventories. We also underestimate the magnitude of observed AOD in the region, at least compared to this specific satellite product. Recent emission trends are less well constrained by observations in India than e.g. in China. The extent to which the model-observation difference arises from the input of anthropogenic emissions or could be influenced by poor model representation of other aerosols sources or atmospheric processes, is not clear from the present analysis. For other regions considered, there is generally agreement in the sign of the simulated area averaged AOD trend between the three sets of simulations, although the magnitude can differ, in particular for the AOD of individual species. For instance, there is an increasing (over time) divergence in the sulfate AOD over Africa between simulations using CEDS and ECLv6. ~~;~~Over most regions, nitrate AOD increases, however, ~~-~~nitrate contribute relatively less to total AOD than sulfate and OA.

Using offline radiative transfer calculations, we estimate a global mean net aerosol RF in 2014 relative to 1990 of 0.03 W m^{-2} for CEDS, 0.08 W m^{-2} for CEDS21, and 0.12 W m^{-2} for ECLv6. ~~Following the continued declined in CEDS21 emissions, a positive global-mean net RF is also estimated for the 5-year period 2014-2019, with the strongest positive signals over China and easter US.~~ Regionally, the sign of the net aerosol-induced RF switched from negative to positive when replacing CEDS emissions with CEDS21 or ECLv6 in our study. Hence, the failure to capture recent observed emission trends in China may have resulted in the wrong sign in estimates of the regional effect on the energy balance over recent decades. Over South Asia, the area average net RF is up to 40% lower in simulations with the updated inventories compared to CEDS.

While the focus of the present study is on anthropogenic aerosols, our comparison with observed AOD reveals potential issues related to the representation of natural aerosols or other processes in the OsloCTM3. ~~Specifically~~In particular, the model~~ed AOD~~ does not capture the strength of the ~~slight~~ ~~p~~positive AOD ~~global tre~~trend observed over high latitude North America and Russia, likely due to an increase in biomass burning aerosols~~apparent in MODIS-Aqua, with key discrepancies over northern hemisphere biomass burning regions and the Southern Ocean~~. For individual years, we also find a larger underestimation in AOD compared to AERONET measurements when switching from CEDS to the

lower CEDS21 and ECLv6 emissions, despite better representation of some key regional observed trends. Further ~~This could indicate that too high anthropogenic emission estimates have masked challenges with for instance dust emissions. Dedicated~~ studies are required to investigate this in more detail.

Anthropogenic aerosols are changing rapidly, particularly in Asia, with potentially large but insufficiently quantified implications for regional climate. We have demonstrated that differences between recent emission inventories translates to notable differences in global and regional trends in anthropogenic aerosol distributions~~can have marked effects on the magnitude and trend of regional and global aerosol abundances~~, and in turn i~~o~~n estimates of radiative forcing. Although additional studies are required to fully quantify the broader implications for aerosol-induced climate and health impacts, our results facilitate comparisons between existing and upcoming studies, using different emission inventories, of anthropogenic aerosols and their effects.

Code availability

The OsloCTM3 is available on from https://github.com/NordicESMhub/OsloCTM3.

Data availability

Model data underlying the manuscript figures are available from 10.6084/m9.figshare.20254764. AERONET data is downloaded from https://aeronet.gsfc.nasa.gov/, MODIS data from https://giovanni.gsfc.nasa.gov/giovanni/, and CEDS21 emissions from the PNNL DataHub https://doi.org/10.25584/PNNLDataHub/1779095.

Acknowledgements

This work has been conducted with support from the Research Council of Norway (grants 248834, 314997 and 324182). The authors acknowledge the UNINETT Sigma2 – the National Infrastructure for High Performance Computing and Data Storage in Norway – resources (grant NN9188K).

Author contributions

MTL led the study design and analysis and the writing. The OsloCTM3 model experiments were performed by MTL and RBS. GM performed the radiative transfer modeling and BHS contributed graphics, silly jokes, and MODIS analysis. All authors contributed to the discussions and writing.

Competing interests

The authors declare that they have no conflict of interest.

References

, !!! INVALID CITATION !!! (e.g. Bauer et al., 2007; Bellouin et al., 2011).

Bauer S. E., Koch D., Unger N., Metzger S. M., Shindell D. T. & Streets D. G. Nitrate aerosols today and in 2030: a global simulation including aerosols and tropospheric ozone, *Atmospheric Chemistry and Physics.* 7(19), 5043-5059, 2007.

Bauer S. E., Tsigaridis K., Faluvegi G., Kelley M., Lo K. K., Miller R. L., Nazarenko L., Schmidt G. A. & Wu J. Historical (1850–2014) Aerosol Evolution and Role on Climate Forcing Using the GISS ModelE2.1 Contribution to CMIP6, *Journal of Advances in Modeling Earth Systems.* 12(8), e2019MS001978, https://doi.org/10.1029/2019MS001978, 2020.

Bellouin N., Rae J., Jones A., Johnson C., Haywood J. & Boucher O. Aerosol forcing in the Climate Model Intercomparison Project (CMIP5) simulations by HadGEM2-ES and the role of ammonium nitrate, *Journal of Geophysical Research-Atmospheres.* 116, D20206, 10.1029/2011jd016074, 2011.

Bellouin N., Quaas J., Gryspeerdt E., Kinne S., Stier P., Watson-Parris D., Boucher O., Carslaw K. S., Christensen M., Daniau A.-L., Dufresne J.-L., Feingold G., Fiedler S., Forster P., Gettelman A., Haywood J. M., Lohmann U., Malavelle F., Mauritsen T., McCoy D. T., Myhre G., Mülmenstädt J., Neubauer D., Possner A., Rugenstein M., Sato Y., Schulz M., Schwartz S. E., Sourdeval O., Storelvmo T., Toll V., Winker D. & Stevens B. Bounding Global Aerosol Radiative Forcing of Climate Change, *Reviews of Geophysics.* 58(1), e2019RG000660, https://doi.org/10.1029/2019RG000660, 2020.

Bian H., Chin M., Hauglustaine D. A., Schulz M., Myhre G., Bauer S. E., Lund M. T., Karydis V. A., Kucsera T. L., Pan X., Pozzer A., Skeie R. B., Steenrod S. D., Sudo K., Tsigaridis K., Tsimpidi A. P. & Tsyro S. G. Investigation of global particulate nitrate from the AeroCom phase III experiment, *Atmos. Chem. Phys.* 17(21), 12911-12940, 10.5194/acp-17-12911-2017, 2017.

Bollasina M. A., Ming Y. & Ramaswamy V. Anthropogenic Aerosols and the Weakening of the South Asian Summer Monsoon, *Science.* 334(6055), 502-505, doi:10.1126/science.1204994, 2011.

Chen S., Zhang X., Lin J., Huang J., Zhao D., Yuan T., Huang K., Luo Y., Jia Z., Zang Z., Qiu Y. a. & Xie L. Fugitive Road Dust PM2.5 Emissions and Their Potential Health Impacts, *Environmental Science & Technology.* 53(14), 8455-8465, 10.1021/acs.est.9b00666, 2019.

Cheng J., Tong D., Liu Y., Yu S., Yan L., Zheng B., Geng G., He K. & Zhang Q. Comparison of Current and Future PM2.5 Air Quality in China Under CMIP6 and DPEC Emission Scenarios, *Geophysical Research Letters.* 48(11), e2021GL093197, https://doi.org/10.1029/2021GL093197, 2021.

Cherian R. & Quaas J. Trends in AOD, Clouds, and Cloud Radiative Effects in Satellite Data and CMIP5 and CMIP6 Model Simulations Over Aerosol Source Regions, *Geophysical Research Letters.* 47(9), e2020GL087132, https://doi.org/10.1029/2020GL087132, 2020.

Chowdhury S., Pozzer A., Haines A., Klingmüller K., Münzel T., Paasonen P., Sharma A., Venkataraman C. & Lelieveld J. Global health burden of ambient PM2.5 and the contribution of anthropogenic black carbon and organic aerosols, *Environment International.* 159, 107020, https://doi.org/10.1016/j.envint.2021.107020, 2022.

Crippa M., Guizzardi D., Muntean M., Schaaf E., Dentener F., van Aardenne J. A., Monni S., Doering U., Olivier J. G. J., Pagliari V. & Janssens-Maenhout G. Gridded emissions of air pollutants for the period 1970–2012 within EDGAR v4.3.2, *Earth Syst. Sci. Data.* 10(4), 1987-2013, 10.5194/essd-10-1987-2018, 2018.

Crippa M., Solazzo E., Huang G., Guizzardi D., Koffi E., Muntean M., Schieberle C., Friedrich R. & Janssens-Maenhout G. High resolution temporal profiles in the Emissions Database for Global Atmospheric Research, *Scientific Data.* 7(1), 121, 10.1038/s41597-020-0462-2, 2020.

Crippa M., Guizzardi D., Butler T., Keating T., Kaminski J., Kuenen, J. , Kurokawa J., Satoru C., Pouliot G., Racine J., Moran M., Klimont Z., Wu R., Manseau P., Barron H., Smith S., Muntean M., Solazzo E., Banja M., Schaaf E., Pagani F., Monforti F. & Pisoni E. HTAPv3 emission mosaic: a global effort to tackle air quality issues, in preparation., 2022.

Elguindi N., Granier C., Stavrakou T., Darras S., Bauwens M., Cao H., Chen C., Denier van der Gon H. A. C., Dubovik O., Fu T. M., Henze D. K., Jiang Z., Keita S., Kuenen J. J. P., Kurokawa J., Liousse C., Miyazaki K., Müller J.-F., Qu Z., Solmon F. & Zheng B. Intercomparison of Magnitudes and Trends

in Anthropogenic Surface Emissions From Bottom-Up Inventories, Top-Down Estimates, and Emission Scenarios, *Earth's Future.* 8(8), e2020EF001520, https://doi.org/10.1029/2020EF001520, 2020.

Forster P., Storelvmo T., Armour K., Collins W., Dufresne J.-L., Frame D., Lunt D. J., Mauritsen T., Palmer M. D., Watanabe M., Wild M. & Zhang H. The Earth's Energy Budget, Climate Feedbacks, and Climate Sensitivity. In Climate Change 2021: The Physical Science Basis. Contribution of Working Group I to the Sixth Assessment Report of the Intergovernmental Panel on Climate Change [Masson-Delmotte, V., P. Zhai, A. Pirani, S.L. Connors, C. Péan, S. Berger, N. Caud, Y. Chen, L. Goldfarb, M.I. Gomis, M. Huang, K. Leitzell, E. Lonnoy, J.B.R. Matthews, T.K. Maycock, T. Waterfield, O. Yelekçi, R. Yu, and B. Zhou (eds.)]. Cambridge University Press, Cambridge, United Kingdom and New York, NY, USA, pp. 923–1054, doi:10.1017/9781009157896.009.

, 2021.

Fricko O., Havlik P., Rogelj J., Klimont Z., Gusti M., Johnson N., Kolp P., Strubegger M., Valin H., Amann M., Ermolieva T., Forsell N., Herrero M., Heyes C., Kindermann G., Krey V., McCollum D. L., Obersteiner M., Pachauri S., Rao S., Schmid E., Schoepp W. & Riahi K. The marker quantification of the Shared Socioeconomic Pathway 2: A middle-of-the-road scenario for the 21st century, *Global Environmental Change.* 42, 251-267, https://doi.org/10.1016/j.gloenvcha.2016.06.004, 2017.

Gliß J., Mortier A., Schulz M., Andrews E., Balkanski Y., Bauer S. E., Benedictow A. M. K., Bian H., Checa-Garcia R., Chin M., Ginoux P., Griesfeller J. J., Heckel A., Kipling Z., Kirkevåg A., Kokkola H., Laj P., Le Sager P., Lund M. T., Lund Myhre C., Matsui H., Myhre G., Neubauer D., van Noije T., North P., Olivié D. J. L., Rémy S., Sogacheva L., Takemura T., Tsigaridis K. & Tsyro S. G. AeroCom phase III multi-model evaluation of the aerosol life cycle and optical properties using ground- and space-based remote sensing as well as surface in situ observations, *Atmos. Chem. Phys.* 21(1), 87-128, 10.5194/acp-21-87-2021, 2021.

Gómez-Sanabria A., Kiesewetter G., Klimont Z., Schoepp W. & Haberl H. Potential for future reductions of global GHG and air pollutants from circular waste management systems, *Nature Communications.* 13(1), 106, 10.1038/s41467-021-27624-7, 2022.

Gui K., Che H., Wang Y., Xia X., Holben B. N., Goloub P., Cuevas-Agulló E., Yao W., Zheng Y., Zhao H., Li L. & Zhang X. A global-scale analysis of the MISR Level-3 aerosol optical depth (AOD) product: Comparison with multi-platform AOD data sources, *Atmospheric Pollution Research.* 12(12), 101238, https://doi.org/10.1016/j.apr.2021.101238, 2021.

Hegerl G. C., Brönnimann S., Cowan T., Friedman A. R., Hawkins E., Iles C., Müller W., Schurer A. & Undorf S. Causes of climate change over the historical record, *Environmental Research Letters.* 14(12), 123006, 10.1088/1748-9326/ab4557, 2019.

Hoesly R. M., Smith S. J., Feng L., Klimont Z., Janssens-Maenhout G., Pitkanen T., Seibert J. J., Vu L., Andres R. J., Bolt R. M., Bond T. C., Dawidowski L., Kholod N., Kurokawa J. I., Li M., Liu L., Lu Z., Moura M. C. P., O'Rourke P. R. & Zhang Q. Historical (1750–2014) anthropogenic emissions of reactive gases and aerosols from the Community Emission Data System (CEDS), *Geosci. Model Dev.* 2018(11), 369-408, https://doi.org/10.5194/gmd-11-369-2018, 2018.

Holben B. N., Eck T. F., Slutsker I., Tanré D., Buis J. P., Setzer A., Vermote E., Reagan J. A., Kaufman Y. J., Nakajima T., Lavenu F., Jankowiak I. & Smirnov A. AERONET—A Federated Instrument Network and Data Archive for Aerosol Characterization, *Remote Sensing of Environment.* 66(1), 1-16, https://doi.org/10.1016/S0034-4257(98)00031-5, 1998.

Kanaya Y., Yamaji K., Miyakawa T., Taketani F., Zhu C., Choi Y., Komazaki Y., Ikeda K., Kondo Y. & Klimont Z. Rapid reduction in black carbon emissions from China: evidence from 2009–2019 observations on Fukue Island, Japan, *Atmos. Chem. Phys.* 20(11), 6339-6356, 10.5194/acp-20-6339-2020, 2020.

Klimont Z., Smith S. J. & Cofala J. The last decade of global anthropogenic sulfur dioxide: 2000–2011 emissions, *Environmental Research Letters.* 8(1), 014003, 10.1088/1748-9326/8/1/014003, 2013.

Klimont Z., Kupiainen K., Heyes C., Purohit P., Cofala J., Rafaj P., Borken-Kleefeld J. & Schöpp W. Global anthropogenic emissions of particulate matter including black carbon, *Atmos. Chem. Phys.* 17(14), 8681-8723, 10.5194/acp-17-8681-2017, 2017.

Korhonen H., Carslaw K. S., Forster P. M., Mikkonen S., Gordon N. D. & Kokkola H. Aerosol climate feedback due to decadal increases in Southern Hemisphere wind speeds, *Geophysical Research Letters.* 37(2), https://doi.org/10.1029/2009GL041320, 2010.

Kurokawa J. & Ohara T. Long-term historical trends in air pollutant emissions in Asia: Regional Emission inventory in ASia (REAS) version 3, *Atmos. Chem. Phys.* 20(21), 12761-12793, 10.5194/acp-20-12761-2020, 2020.

Levy R. C., Remer L. A., Kleidman R. G., Mattoo S., Ichoku C., Kahn R. & Eck T. F. Global evaluation of the Collection 5 MODIS dark-target aerosol products over land, *Atmos. Chem. Phys.* 10(21), 10399-10420, 10.5194/acp-10-10399-2010, 2010.

Li C., McLinden C., Fioletov V., Krotkov N., Carn S., Joiner J., Streets D., He H., Ren X., Li Z. & Dickerson R. R. India Is Overtaking China as the World's Largest Emitter of Anthropogenic Sulfur Dioxide, *Scientific Reports.* 7(1), 14304, 10.1038/s41598-017-14639-8, 2017.

Lund M. T., Myhre G., Haslerud A. S., Skeie R. B., Griesfeller J., Platt S. M., Kumar R., Myhre C. L. & Schulz M. Concentrations and radiative forcing of anthropogenic aerosols from 1750 to 2014 simulated with the Oslo CTM3 and CEDS emission inventory, *Geosci. Model Dev.* 11(12), 4909-4931, 10.5194/gmd-11-4909-2018, 2018.

Lund M. T., Myhre G. & Samset B. H. Anthropogenic aerosol forcing under the Shared Socioeconomic Pathways, *Atmos. Chem. Phys.* 19(22), 13827-13839, 10.5194/acp-19-13827-2019, 2019.

Lund M. T., Aamaas B., Stjern C. W., Klimont Z., Berntsen T. K. & Samset B. H. A continued role of short-lived climate forcers under the Shared Socioeconomic Pathways, *Earth Syst. Dynam.* 11(4), 977-993, 10.5194/esd-11-977-2020, 2020.

Marvel K., Biasutti M. & Bonfils C. Fingerprints of external forcings on Sahel rainfall: aerosols, greenhouse gases, and model-observation discrepancies, *Environmental Research Letters.* 15(8), 084023, 10.1088/1748-9326/ab858e, 2020.

MOD08 MODIS Level 3 Atmosphere Products (MOD 08), Data Products Handbook Volume 2. https://modis.gsfc.nasa.gov/data/dataprod/dataproducts.php?MOD_NUMBER=08 (accessed 04/26/2018), 2018.

Mortier A., Gliß J., Schulz M., Aas W., Andrews E., Bian H., Chin M., Ginoux P., Hand J., Holben B., Zhang H., Kipling Z., Kirkevåg A., Laj P., Lurton T., Myhre G., Neubauer D., Olivié D., von Salzen K., Skeie R. B., Takemura T. & Tilmes S. Evaluation of climate model aerosol trends with ground-based observations over the last 2 decades – an AeroCom and CMIP6 analysis, *Atmos. Chem. Phys.* 20(21), 13355-13378, 10.5194/acp-20-13355-2020, 2020.

Moseid K. O., Schulz M., Storelvmo T., Julsrud I. R., Olivié D., Nabat P., Wild M., Cole J. N. S., Takemura T., Oshima N., Bauer S. E. & Gastineau G. Bias in CMIP6 models as compared to observed regional dimming and brightening, *Atmos. Chem. Phys.* 20(24), 16023-16040, 10.5194/acp-20-16023-2020, 2020.

Myhre G., Samset B. H., Schulz M., Balkanski Y., Bauer S., Berntsen T. K., Bian H., Bellouin N., Chin M., Diehl T., Easter R. C., Feichter J., Ghan S. J., Hauglustaine D., Iversen T., Kinne S., Kirkevåg A., Lamarque J. F., Lin G., Liu X., Lund M. T., Luo G., Ma X., van Noije T., Penner J. E., Rasch P. J., Ruiz A., Seland Ø., Skeie R. B., Stier P., Takemura T., Tsigaridis K., Wang P., Wang Z., Xu L., Yu H., Yu F., Yoon J. H., Zhang K., Zhang H. & Zhou C. Radiative forcing of the direct aerosol effect from AeroCom Phase II simulations, *Atmos. Chem. Phys.* 13(4), 1853-1877, 10.5194/acp-13-1853-2013, 2013.

Myhre G., Aas W., Cherian R., Collins W., Faluvegi G., Flanner M., Forster P., Hodnebrog Ø., Klimont Z., Lund M. T., Mülmenstädt J., Lund Myhre C., Olivié D., Prather M., Quaas J., Samset B. H., Schnell J. L., Schulz M., Shindell D., Skeie R. B., Takemura T. & Tsyro S. Multi-model simulations of aerosol and ozone radiative forcing due to anthropogenic emission changes during the period 1990–2015, *Atmos. Chem. Phys.* 17(4), 2709-2720, 10.5194/acp-17-2709-2017, 2017.

O'Rourke P. R., Smith S. J., Mott A., Ahsan H., McDuffie E. E., Crippa M., Klimont S., McDonald B., Wang Z., Nicholson M. B., Feng L. & Hoesly R. M. (2021), CEDS v-2021-02-05 Emission Data 1975-2019 (Version Feb-05-2021), edited, Zenodo.

Paulot F., Paynter D., Ginoux P., Naik V. & Horowitz L. W. Changes in the aerosol direct radiative forcing from 2001 to 2015: observational constraints and regional mechanisms, *Atmos. Chem. Phys.* 18(17), 13265-13281, 10.5194/acp-18-13265-2018, 2018.

Paulot F., Paynter D., Winton M., Ginoux P., Zhao M. & Horowitz L. W. Revisiting the Impact of Sea Salt on Climate Sensitivity, *Geophysical Research Letters.* 47(3), e2019GL085601, https://doi.org/10.1029/2019GL085601, 2020.

Persad G. G., Samset B. H. & Wilcox L. J. Comment: Aerosols must be included in climate risk assessments, *Nature.* 611, 662-664, 2022.

Quaas J., Boucher O. & Lohmann U. Constraining the total aerosol indirect effect in the LMDZ and ECHAM4 GCMs using MODIS satellite data, *Atmos. Chem. Phys.* 6(4), 947-955, 10.5194/acp-6-947-2006, 2006.

Quaas J., Jia H., Smith C., Albright A. L., Aas W., Bellouin N., Boucher O., Doutriaux-Boucher M., Forster P. M., Grosvenor D., Jenkins S., Klimont Z., Loeb N. G., Ma X., Naik V., Paulot F., Stier P., Wild M., Myhre G. & Schulz M. Robust evidence for reversal in the aerosol effective climate forcing trend, *Atmos. Chem. Phys. Discuss.* 2022, 1-25, 10.5194/acp-2022-295, 2022.

Ramachandran S., Rupakheti M. & Cherian R. Insights into recent aerosol trends over Asia from observations and CMIP6 simulations, *Science of The Total Environment.* 807, 150756, https://doi.org/10.1016/j.scitotenv.2021.150756, 2022.

Randerson J. T., van der Werf G. R., Giglio L., Collatz G. J. & Kasibhatla P. S. Global Fire Emissions Database, Version 4.1 (GFEDv4). ORNL DAAC, Oak Ridge, Tennessee, USA. , https://doi.org/10.3334/ORNLDAAC/1293, 2017.

Regayre L. A., Pringle K. J., Booth B. B. B., Lee L. A., Mann G. W., Browse J., Woodhouse M. T., Rap A., Reddington C. L. & Carslaw K. S. Uncertainty in the magnitude of aerosol-cloud radiative forcing over recent decades, *Geophysical Research Letters.* 41(24), 9040-9049, https://doi.org/10.1002/2014GL062029, 2014.

Samset B. H., Sand M., Smith C. J., Bauer S. E., Forster P. M., Fuglestvedt J. S., Osprey S. & Schleussner C.-F. Climate Impacts From a Removal of Anthropogenic Aerosol Emissions, *Geophysical Research Letters.* 45(2), 1020-1029, https://doi.org/10.1002/2017GL076079, 2018.

Samset B. H., Lund M. T., Bollasina M., Myhre G. & Wilcox L. Emerging Asian aerosol patterns, *Nature Geoscience.* 12(8), 582-584, 10.1038/s41561-019-0424-5, 2019.

SCPRC The State Council Issues Action Plan on Prevention and Control of Air Pollution Introducing Ten Measures to Improve Air Quality. https://english.mee.gov.cn/News_service/infocus/201309/t20130924_260707.shtm (Accessed 22/01/20), 2013.

SCPRC The State Council rolls out a three-year action plan for clean air. https://english.mee.gov.cn/News_service/news_release/201807/t20180713_446624.shtml (Accessed 22/01/20), 2018.

Sherman J. P., Gupta P., Levy R. C. & Sherman P. J. An Evaluation of MODIS-Retrieved Aerosol Optical Depth over a Mountainous AERONET Site in the Southeastern US, *Aerosol and Air Quality Research.* 16(12), 3243-3255, 10.4209/aaqr.2015.09.0568, 2017.

Sillmann J., Pozzoli L., Vignati E., Kloster S. & Feichter J. Aerosol effect on climate extremes in Europe under different future scenarios, *Geophysical Research Letters.* 40(10), 2290-2295, https://doi.org/10.1002/grl.50459, 2013.

Smith S. J., McDuffie E. E. & Charles M. Opinion: Coordinated development of emission inventories for climate forcers and air pollutants, *Atmos. Chem. Phys.* 22(19), 13201-13218, 10.5194/acp-22-13201-2022, 2022.

Stamnes K., Tsay S. C., Wiscombe W. & Jayaweera K. Numerically stable algorithm for discrete-ordinate-method radiative transfer in multiple scattering and emitting layered media, *Appl. Opt.* 27(12), 2502-2509, 10.1364/AO.27.002502, 1988.

Struthers H., Ekman A. M. L., Glantz P., Iversen T., Kirkevåg A., Seland Ø., Mårtensson E. M., Noone K. & Nilsson E. D. Climate-induced changes in sea salt aerosol number emissions: 1870 to 2100, *Journal of Geophysical Research: Atmospheres.* 118(2), 670-682, https://doi.org/10.1002/jgrd.50129, 2013.

Su W., Liang L., Myhre G., Thorsen T. J., Loeb N. G., Schuster G. L., Ginoux P., Paulot F., Neubauer D., Checa-Garcia R., Matsui H., Tsigaridis K., Skeie R. B., Takemura T., Bauer S. E. & Schulz M. Understanding Top-of-Atmosphere Flux Bias in the AeroCom Phase III Models: A Clear-Sky Perspective, *Journal of Advances in Modeling Earth Systems.* 13(9), e2021MS002584, https://doi.org/10.1029/2021MS002584, 2021.

Szopa S., Naik V., Adhikary B., Artaxo P., Berntsen T., Collins W. D., Fuzzi S., Gallardo L., Kiendler Scharr A., Klimont Z., Liao H., Unger N. & Zanis P. Short-Lived Climate Forcers. In: Climate Change 2021: The Physical Science Basis. Contribution of Working Group I to the Sixth Assessment Report of the Intergovernmental Panel on Climate Change [Masson-Delmotte, V., P. Zhai, A. Pirani, S. L. Connors, C. Péan, S. Berger, N. Caud, Y. Chen, L. Goldfarb, M. I. Gomis, M. Huang, K. Leitzell, E. Lonnoy, J. B. R. Matthews, T. K. Maycock, T. Waterfield, O. Yelekçi, R. Yu and B. Zhou (eds.)]. Cambridge University Press, Cambridge, United Kingdom and New York, NY, USA, pp. 817–922 doi:10.1017/9781009157896.008, 2021.

Søvde O. A., Prather M. J., Isaksen I. S. A., Berntsen T. K., Stordal F., Zhu X., Holmes C. D. & Hsu J. The chemical transport model Oslo CTM3, *Geosci. Model Dev.* 5(6), 1441-1469, 10.5194/gmd-5-1441-2012, 2012.

Tong D., Cheng J., Liu Y., Yu S., Yan L., Hong C., Qin Y., Zhao H., Zheng Y., Geng G., Li M., Liu F., Zhang Y., Zheng B., Clarke L. & Zhang Q. Dynamic projection of anthropogenic emissions in China: methodology and 2015–2050 emission pathways under a range of socio-economic, climate policy, and pollution control scenarios, *Atmos. Chem. Phys.* 20(9), 5729-5757, 10.5194/acp-20-5729-2020, 2020.

van Marle M. J. E., Kloster S., Magi B. I., Marlon J. R., Daniau A. L., Field R. D., Arneth A., Forrest M., Hantson S., Kehrwald N. M., Knorr W., Lasslop G., Li F., Mangeon S., Yue C., Kaiser J. W. & van der Werf G. R. Historic global biomass burning emissions for CMIP6 (BB4CMIP) based on merging satellite observations with proxies and fire models (1750–2015), *Geosci. Model Dev.* 10(9), 3329-3357, 10.5194/gmd-10-3329-2017, 2017.

Vogel A., Alessa G., Scheele R., Weber L., Dubovik O., North P. & Fiedler S. Uncertainty in Aerosol Optical Depth From Modern Aerosol-Climate Models, Reanalyses, and Satellite Products, *Journal of Geophysical Research: Atmospheres.* 127(2), e2021JD035483, https://doi.org/10.1029/2021JD035483, 2022.

Wang C.-S., Wang Z.-L., Lei Y.-D., Zhang H., Che H.-Z. & Zhang X.-Y. Differences in East Asian summer monsoon responses to Asian aerosol forcing under different emission inventories, *Advances in Climate Change Research*, https://doi.org/10.1016/j.accre.2022.02.008, 2022.

Wang Z., Lin L., Xu Y., Che H., Zhang X., Zhang H., Dong W., Wang C., Gui K. & Xie B. Incorrect Asian aerosols affecting the attribution and projection of regional climate change in CMIP6 models, *npj Climate and Atmospheric Science.* 4(1), 2, 10.1038/s41612-020-00159-2, 2021.

Wiedinmyer C., Yokelson R. J. & Gullett B. K. Global Emissions of Trace Gases, Particulate Matter, and Hazardous Air Pollutants from Open Burning of Domestic Waste, *Environmental Science & Technology.* 48(16), 9523-9530, 10.1021/es502250z, 2014.

Womack C. C., McDuffie E. E., Edwards P. M., Bares R., de Gouw J. A., Docherty K. S., Dubé W. P., Fibiger D. L., Franchin A., Gilman J. B., Goldberger L., Lee B. H., Lin J. C., Long R., Middlebrook A. M., Millet D. B., Moravek A., Murphy J. G., Quinn P. K., Riedel T. P., Roberts J. M., Thornton J. A., Valin L. C., Veres P. R., Whitehill A. R., Wild R. J., Warneke C., Yuan B., Baasandorj M. & Brown S. S. An Odd Oxygen Framework for Wintertime Ammonium Nitrate Aerosol Pollution in Urban Areas: NOx and VOC Control as Mitigation Strategies, *Geophysical Research Letters.* 46(9), 4971-4979, https://doi.org/10.1029/2019GL082028, 2019.

Wu C., Venevsky S., Sitch S., Mercado L. M., Huntingford C. & Staver A. C. Historical and future global burned area with changing climate and human demography, *One Earth.* 4(4), 517-530, https://doi.org/10.1016/j.oneear.2021.03.002, 2021.

Xia W., Wang Y., Chen S., Huang J., Wang B., Zhang G. J., Zhang Y., Liu X., Ma J., Gong P., Jiang Y., Wu M., Xue J., Wei L. & Zhang T. Double Trouble of Air Pollution by Anthropogenic Dust, *Environmental Science & Technology.* 56(2), 761-769, 10.1021/acs.est.1c04779, 2022.

Yang S., Yuan B., Peng Y., Huang S., Chen W., Hu W., Pei C., Zhou J., Parrish D. D., Wang W., He X., Cheng C., Li X. B., Yang X., Song Y., Wang H., Qi J., Wang B., Wang C., Wang C., Wang Z., Li T., Zheng E., Wang S., Wu C., Cai M., Ye C., Song W., Cheng P., Chen D., Wang X., Zhang Z., Wang X., Zheng J. & Shao M. The formation and mitigation of nitrate pollution: comparison between urban and suburban environments, *Atmos. Chem. Phys.* 22(7), 4539-4556, 10.5194/acp-22-4539-2022, 2022.

Zhai S., Jacob D. J., Wang X., Liu Z., Wen T., Shah V., Li K., Moch J. M., Bates K. H., Song S., Shen L., Zhang Y., Luo G., Yu F., Sun Y., Wang L., Qi M., Tao J., Gui K., Xu H., Zhang Q., Zhao T., Wang Y., Lee H. C., Choi H. & Liao H. Control of particulate nitrate air pollution in China, *Nature Geoscience.* 14(6), 389-395, 10.1038/s41561-021-00726-z, 2021.

Zheng B., Tong D., Li M., Liu F., Hong C., Geng G., Li H., Li X., Peng L., Qi J., Yan L., Zhang Y., Zhao H., Zheng Y., He K. & Zhang Q. Trends in China's anthropogenic emissions since 2010 as the consequence of clean air actions, *Atmos. Chem. Phys.* 18(19), 14095-14111, 10.5194/acp-18-14095-2018, 2018.

Aas W., Mortier A., Bowersox V., Cherian R., Faluvegi G., Fagerli H., Hand J., Klimont Z., Galy-Lacaux C., Lehmann C. M. B., Myhre C. L., Myhre G., Olivié D., Sato K., Quaas J., Rao P. S. P., Schulz M., Shindell D., Skeie R. B., Stein A., Takemura T., Tsyro S., Vet R. & Xu X. Global and regional trends of atmospheric sulfur, *Scientific Reports.* 9(1), 953, 10.1038/s41598-018-37304-0, 2019.

Tables:

Table 1: Summary of experiments used in the study.

Name	Description	Years simulated
CEDS	CEDS v2016 emissions, fixed meteorology	1990, 1995, 2000, 2005, 2010 2014
CEDS21	CEDS v2021 emissions, fixed meteorology	1990, 1995, 2000, 2005, 2010 2014, 2016, 2018, 2019
ECLv6	ECLIPSEv6b emissions, fixed meteorology	1990, 1995, 2000, 2005, 2010 2014, 2016
CEDSmet	CEDS v2017 emissions until 2014 and SSP2-4.5 for 2015-2017, running meteorology	1990-2017
CEDS21met	CEDS v2021 emissions, running meteorology	2001-2017

Figures:

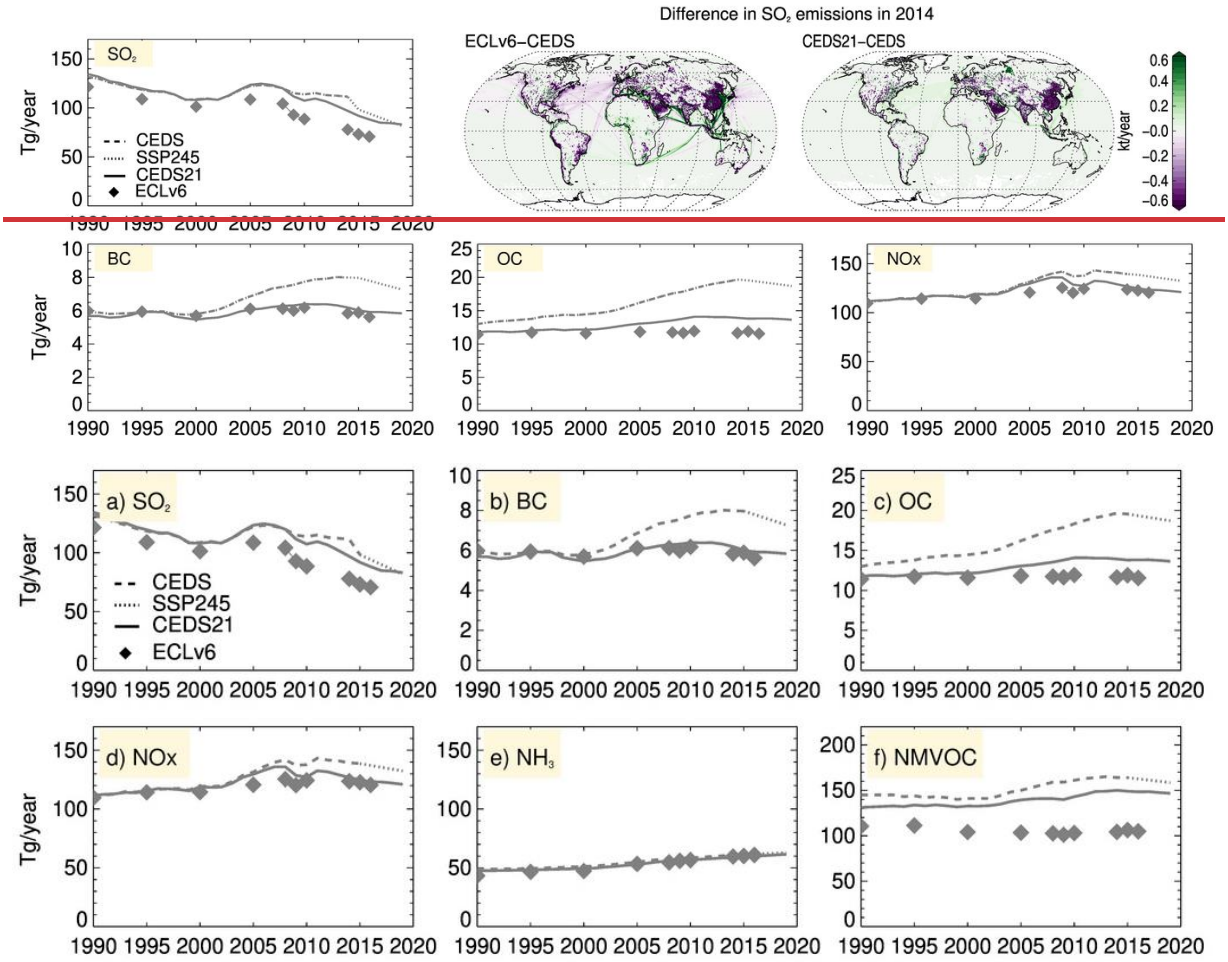

Figure 1 *Global total anthropogenic emissions of SO_2, BC, OC, ~~and~~ NOx, NH_3, and NMVOC in the CEDS21, ECLv6, CEDS17 inventories, for the period 1990 to the most recent inventory year (2019, 2016 and 2014, respectively). Dotted lines show emissions from the SSP2-4.5 scenario, linearly interpolated from 2015 to 2019.* ~~*The maps show the difference in SO_2 emissions in 2014, the most recent common year*~~

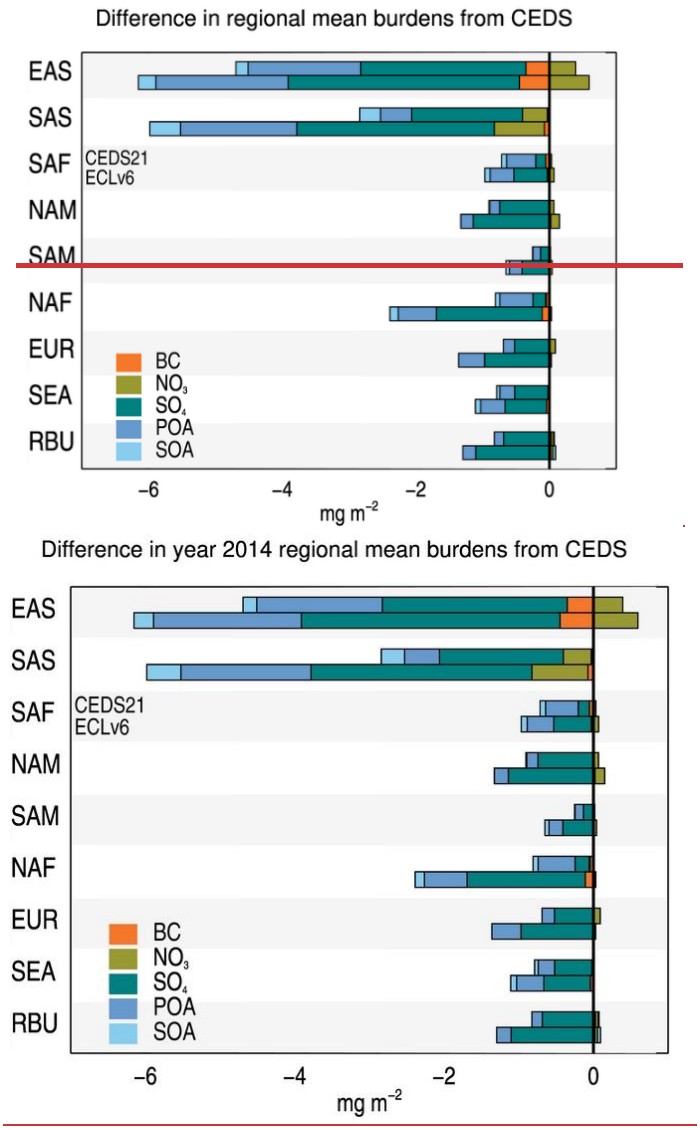

Figure 2 *Absolute difference in regional mean burden of the key anthropogenic aerosol species between simulations with CEDS21 and CEDS (upper bar) and ECLv6 and CEDS (lower bar). Regions are the same as in Lund et al. (2019): EAS = East Asia, SAS = South Asia, SAF = Sub-Saharan Africa, NAM = North America, SAM = South America, NAF = North Africa and the Middle East, EUR = Europe, SEA = South East Asia, RBU = Russia.*

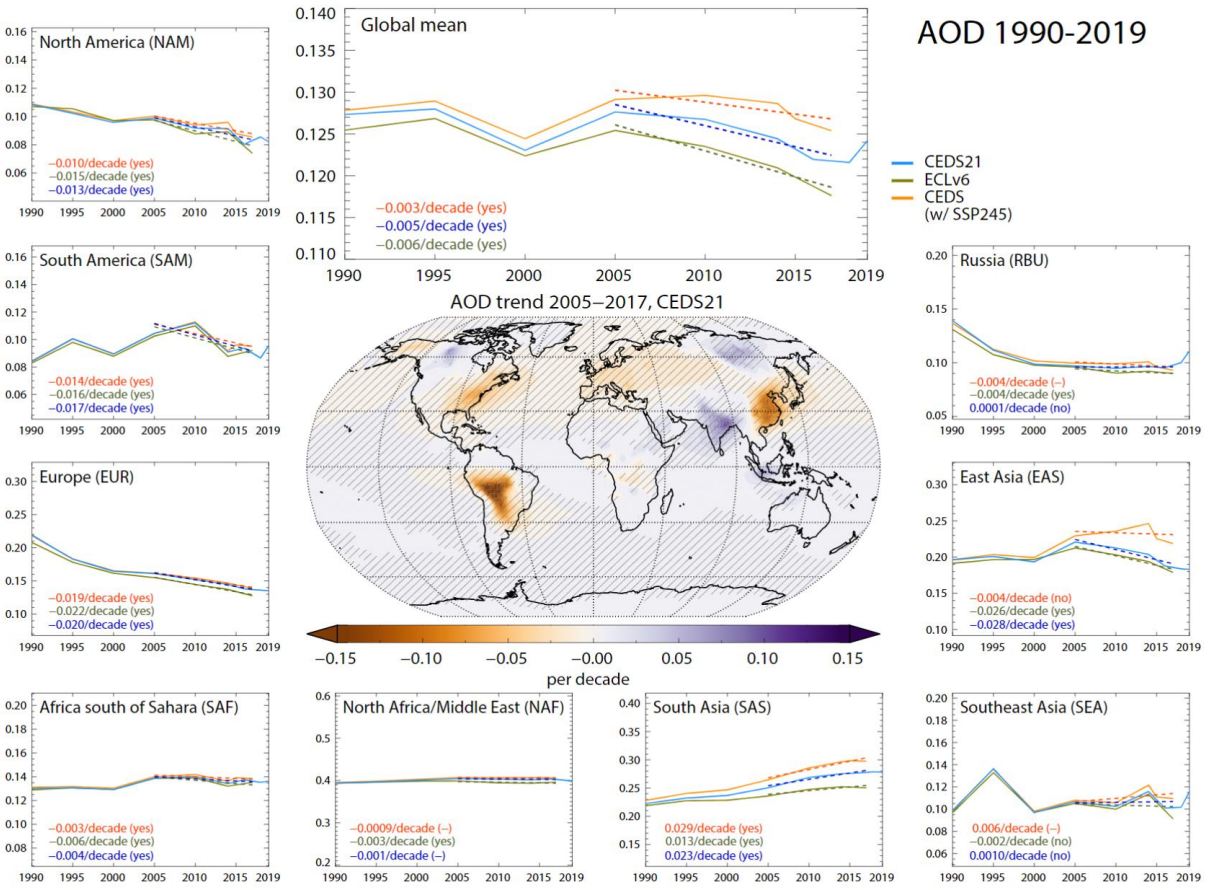
AOD 1990-2019
Global mean
−0.003/decade (yes)
−0.005/decade (yes)
−0.006/decade (yes)
CEDS21
ECLv6
CEDS
(w/ SSP245)
North America (NAM)
−0.010/decade (yes)
−0.015/decade (yes)
−0.013/decade (yes)
South America (SAM)
−0.014/decade (yes)
−0.016/decade (yes)
−0.017/decade (yes)
Europe (EUR)
−0.019/decade (yes)
−0.022/decade (yes)
−0.020/decade (yes)
AOD trend 2005–2017, CEDS21
−0.15 −0.10 −0.05 −0.00 0.05 0.10 0.15
per decade
Russia (RBU)
−0.004/decade (−)
−0.004/decade (yes)
0.0001/decade (no)
East Asia (EAS)
−0.004/decade (no)
−0.026/decade (yes)
−0.028/decade (yes)
Africa south of Sahara (SAF)
−0.003/decade (yes)
−0.006/decade (yes)
−0.004/decade (yes)
North Africa/Middle East (NAF)
−0.0009/decade (−)
−0.003/decade (yes)
−0.001/decade (−)
South Asia (SAS)
0.029/decade (yes)
0.013/decade (yes)
0.023/decade (yes)
Southeast Asia (SEA)
0.006/decade (−)
−0.002/decade (no)
0.0010/decade (no)

1238

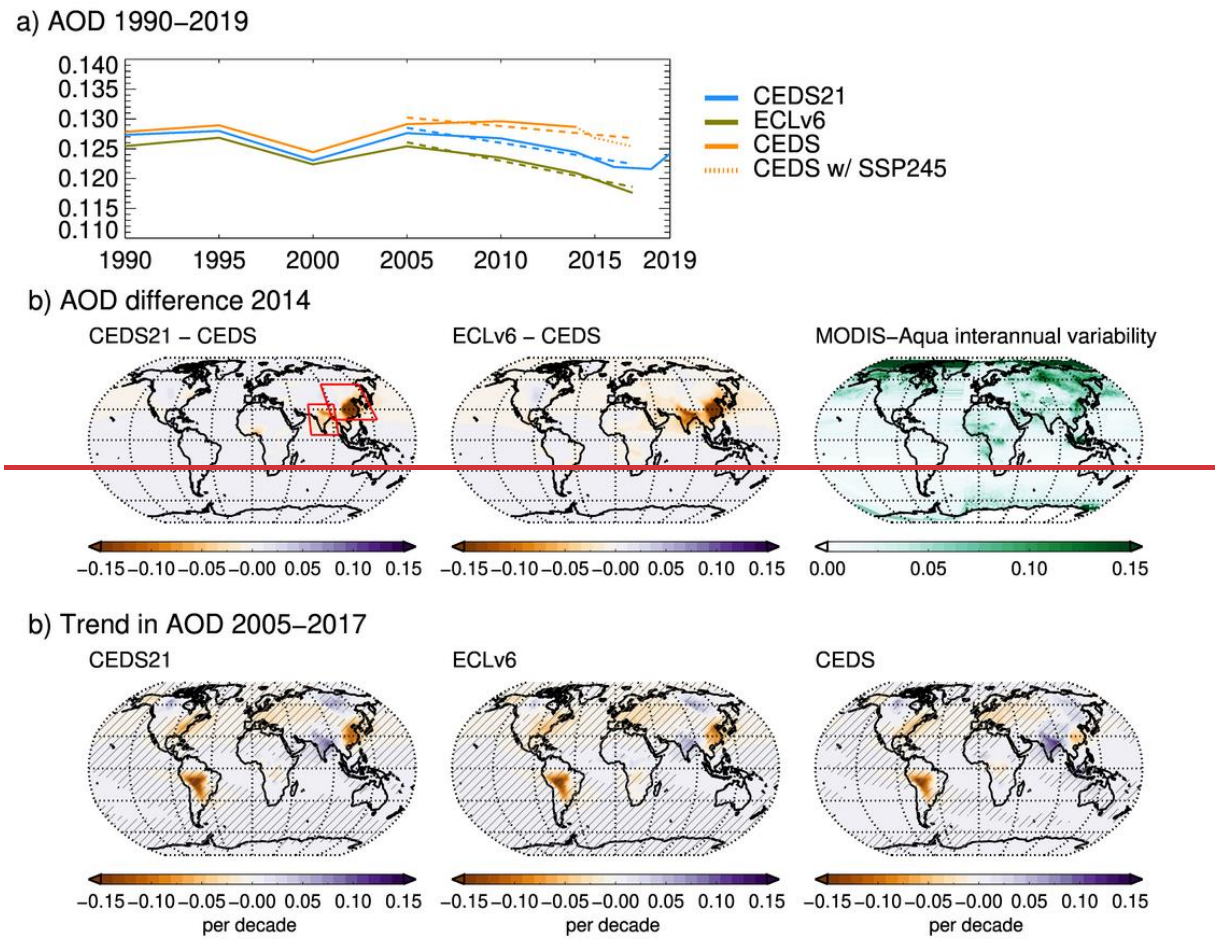

Figure 3: ~~a)~~ Global and regional mean total AOD simulated with emissions from the CEDS21, ECLv6 and CEDS inventories. In the case of CEDS, the timeseries is extended from 2014 to 2017 using SSP2-4.5 emissions. Dashed lines show the linear 2005-2017 trend, defined as statistically significant from no trend when the linear Pearsons correlation coefficient is significant at the 0.05 level. To reduce any influence of individual, outlier years on the trends, we calculate a set of trends removing one-and-one year from the sample and show the average. Significance is given in the parenthesis. If a dash is given, individual trends from the sample differed from each other in terms of significance. ~~b) Difference in AOD between the two inventories and CEDS in 2014, i.e. the last year of historical emissions in CEDS. Also shown is the interannual variability in MODIS AOD. c) Regional linear trends in AOD over 2005-2017 with the three different emission inventories.~~

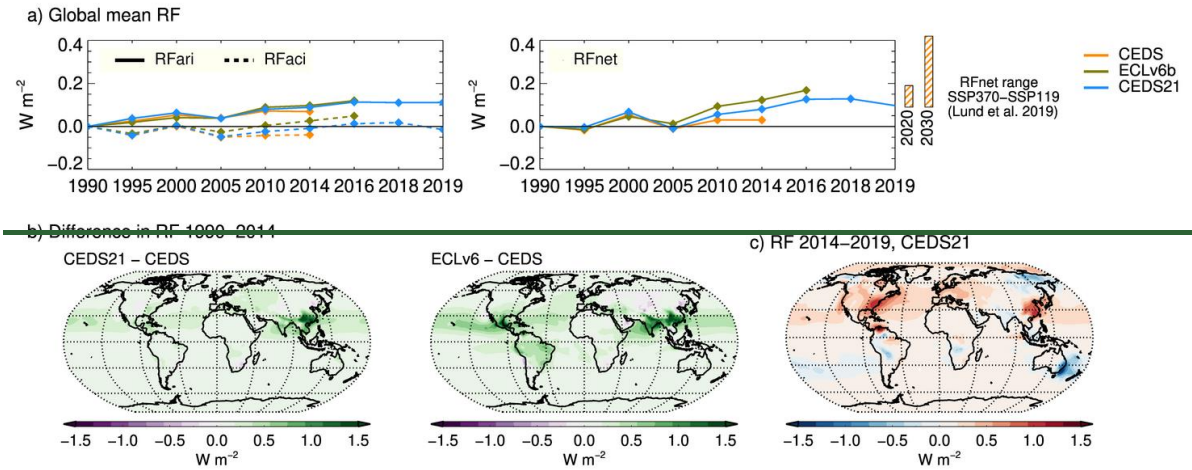

~~Figure 4: a) RFari and RFaci (left) and RFnet (RFari+RFaci) relative to 1990 under the CEDS21, ECLv6, and CEDS emission inventories. The vertical bars to the right show the range in RFnet in 2020 and 2030 (relative to 1990) estimated with the SSP1-1.9 and SSP3-7.0 emissions (adapted from Lund et al. (2019)). b) Difference in RFnet in 2014 relative to 1990 between simulations with ECLv6 and CEDS emissions. c) The RFnet in 2019 relative to 2014 with CEDS21.~~

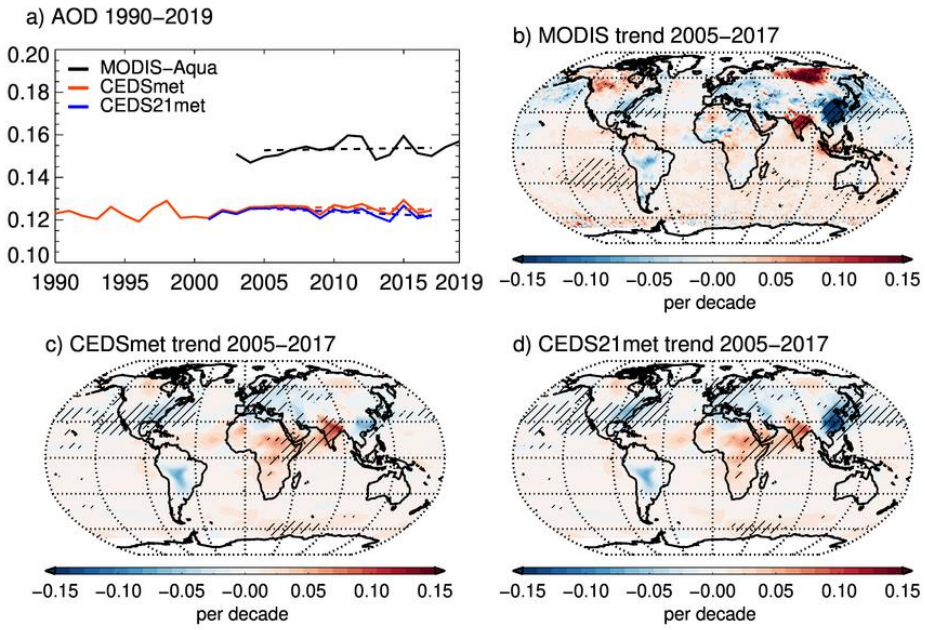

Figure ~~45~~: a) Global, annual mean AOD from MODIS-Aqua and the OsloCTM3 over the 1990-2019 period. Note that data north and south of 70° is excluded here due to the limited MODIS-Aqua coverage. Dashed lines show linear trend from 2005 to 2017. b-d) Spatially resolved linear trends in observed and simulated AOD. Hatching indicates where the linear trend is significantly different from zero at the 0.05 level.

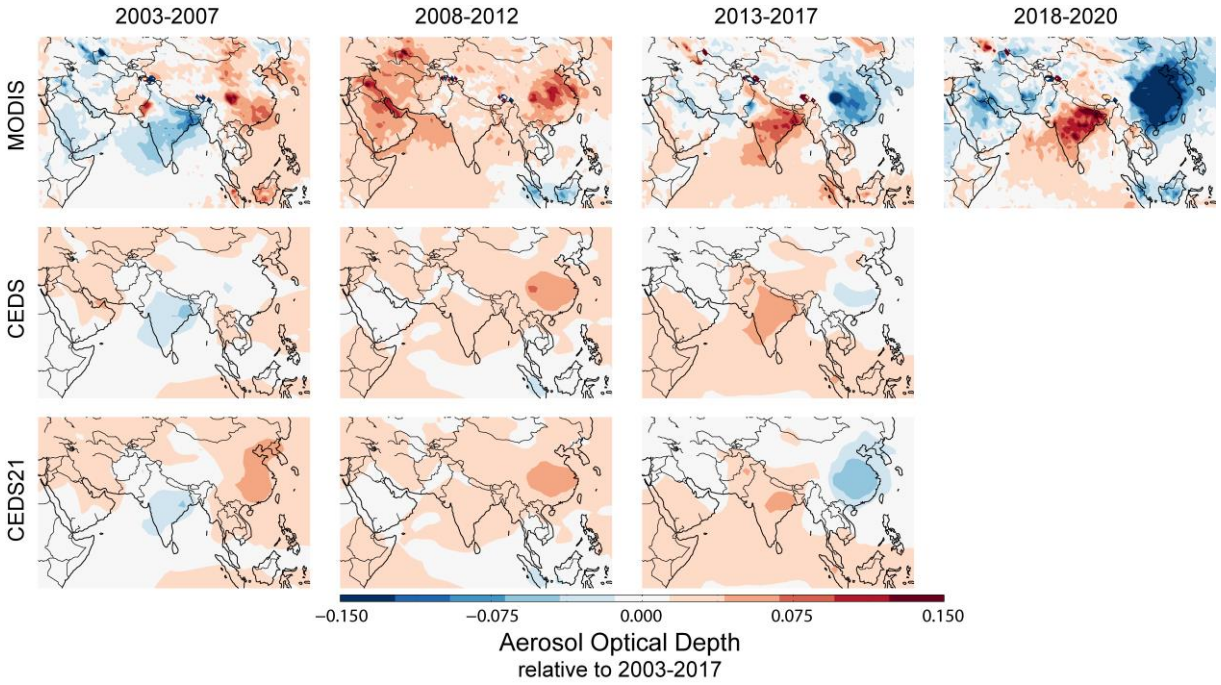

Figure 5~~6~~: Evolution of AOD over South and East Asia, and the Middle East, over the period 2003-2020. All panels show five-year average deviations from the period 2003-2017, except the rightmost MODIS-Aqua panel which show the three-year average deviation (same baseline). The top row shows retrievals from MODIS Aqua; the two bottom rows show model calculations with OsloCTM3 based on the CEDS and CEDS21 emission inventories.

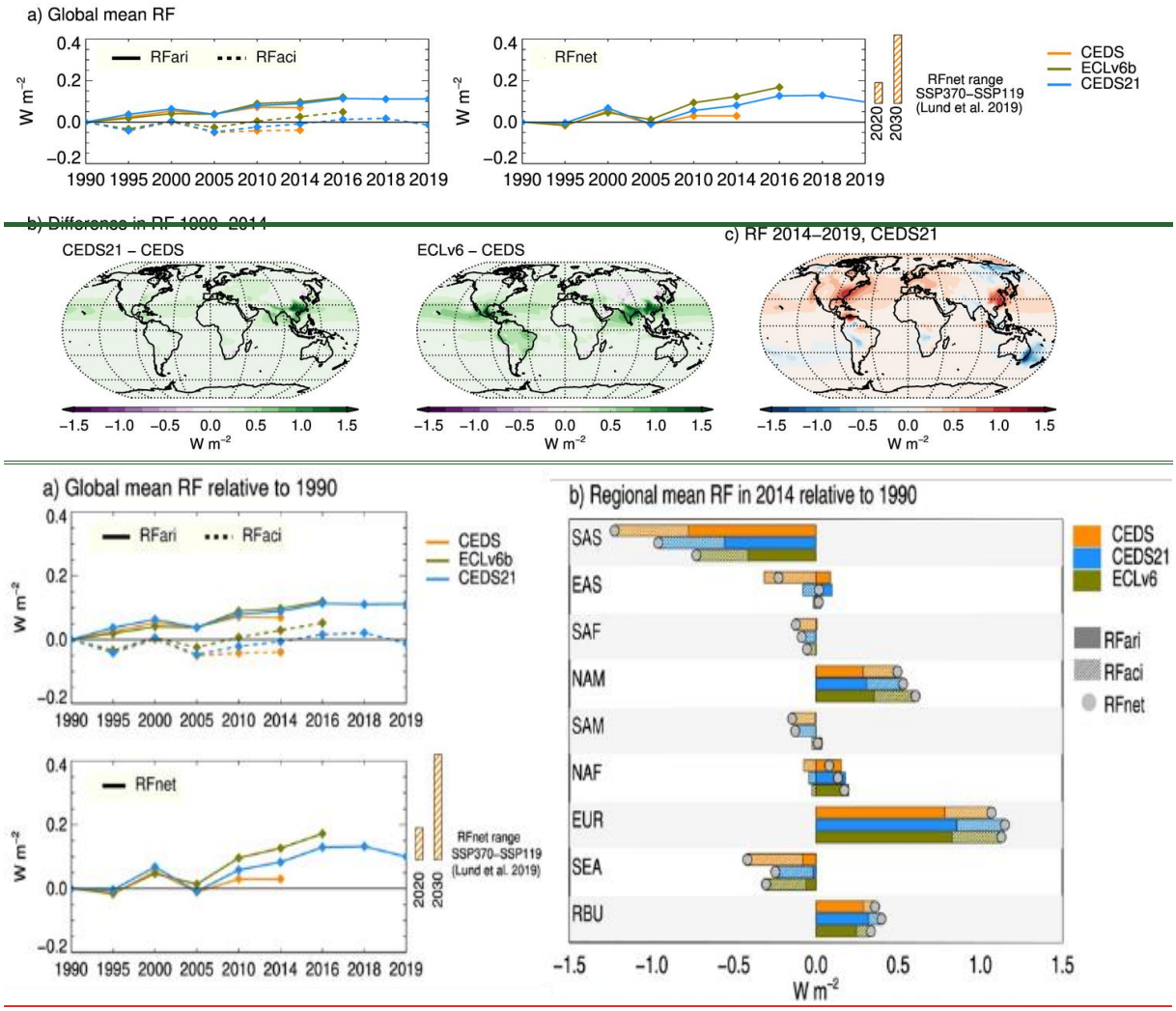

Figure 46: a) Global mean RFari and RFaci (top~~left~~) and RFnet (RFari+RFaci) (bottom) relative to 1990 from simulations ~~under~~ using ~~t~~the CEDS, CEDS21, and ECLv6~~, and CEDS~~ emission inventories. The vertical bars to the right show the range in RFnet in 2020 and 2030 (relative to 1990) estimated with the SSP1-1.9 and SSP3-7.0 emissions (adapted from Lund et al. (2019)). b) Regional mean RFnet, RFari, and RFaci in ~~Difference in RFnet in~~ 2014 relative to 1990 ~~between~~in simulations with CEDS, CEDS21, and ECLv6 ~~and CEDS~~ inventories~~emissions. c) The RFnet in 2019 relative to 2014 with CEDS21.~~